

Geochemical Evidence for the Origin of Mineralogical
Rinds Surrounding Garnet-Amphibolite Blocks in a
Subduction Zone Mélange, Catalina Island, California

Lauren J. Magliozzi

Submitted to the Department of Chemistry
of Smith College
in partial fulfillment
of the requirements for the degree of
Bachelor of Arts with Honors

John B. Brady, Honors Project Advisor
May 2013

Abstract

Mineralogical rinds surround garnet-amphibolite blocks in a subduction zone mélange on Catalina Island, California. The rinds, which occur in concentric layers, are composed of different amphiboles and similar garnets to those in the garnet+amphibole+rutile blocks. Analyses of compositional chemistry was applied to understanding the mechanism of formation of such mineralogical rinds to examine the role of mechanical mixing, fluid metasomatism, and chemical diffusion. An examination of the mineralogy and chemistry of the samples support a model of high temperature amphibolite blocks chemically diffusing with a contrasting serpentinite matrix at lower temperatures in the presence of a water-rich fluid. Mechanical mixing, as suggested by previous studies on the Catalina Schist, cannot explain the presence of multiple rind layers.

TABLE OF CONTENTS

Abstract	2
Acknowledgements	4
Introduction	5
Background information	
Santa Catalina Island.....	5
Subduction Zones.....	8
Metamorphism and Facies.....	9
Previous Work on the Catalina Schist.....	16
Objectives.....	21
Fluids and Metasomatism.....	21
Mechanical Mixing.....	23
Diffusion Reactions of Solids.....	23
Amphibole Structure.....	25
Garnet Structure.....	27
Methods	
Field Methods.....	29
Optical Light Microscopy.....	30
Scanning Electron Microscopy and Energy-dispersive X-Ray Spectroscopy.....	31
Thermometry.....	32
Results	
Sample Descriptions.....	34
Compositional Chemistry.....	52
Discussion	55
Conclusions	62
References	63
Appendix	65

Acknowledgements

I would like to thank John Brady for his truly tireless work, dedication, and encouragement throughout this project and throughout my time as a student at Smith. His scientific and personal guidance has been invaluable and I'm truly lucky to have worked with such a great scientist and mentor. I'd like to recognize Clémentine Hamelin '15 for her work in the lab with me. I'd also like to thank Carrie Read both for sticking with me through this project (no matter how geological and unrelated to her specialties it is), and also for helping me to find a bridge between materials chemistry and mineralogy through her research. I'd like to thank my five KECK research peers who accompanied me to Catalina Island and lived with me for an entire month in the field working, camping, cooking, hiking, and laughing beside me. I'd like to thank my friends Michelle Cortrite and Amanda Macavoy for always being there for me and helping me, especially with finding the courage to present my work to others. And finally, I'd like to thank my parents for supporting me and for instilling in me a love of small wonders at a young age.



**Keck Consortium Fellowship Researchers on Catalina Island, CA
July 2012**

Introduction

Catalina Island off the coast of Los Angeles, California is host to metamorphic rocks formed at a variety of temperatures and pressures. While the area is known for its tectonic history as a subduction zone, metamorphic rocks of higher temperatures than those characteristic of subduction zones are present, such as garnet-amphibolites.

Moreover, some of the garnet-amphibolite blocks found amongst dissimilar material as isolated, exotic rock units, are encased by mineralogically distinct rind layers. The formation of such rinds has been attributed to a variety of mechanisms including fluid metasomatism, mechanical mixing, and chemical diffusion. This thesis focuses on the mineralogical rinds surrounding amphibolite blocks and provides geochemical evidence bearing on the possible mechanisms of their formation.

Santa Catalina Island



Figure 1. Geographic location of Catalina Island, California with Ripper's Cove marked. Samples in this study are from Ripper's Cove.



Figure 2. Ripper's Cover, Catalina Island peppered with blocks.

Catalina Island is located near the coast of southern California, just south of Los Angeles (Fig. 1). The Catalina Schist is a rock unit that outcrops on the island that has received attention for its complicated tectonometamorphic history. Tectonically, it has been described as a subduction zone assemblage with a mix of island arc igneous and sedimentary origins (Grove et al., 2008). These arrangements have been studied for decades as a natural laboratory of geochemical evolution within a subduction zone setting. (Platt, 1975; Sorenson, 1987; Bebout 1989).

Isolated blocks of garnet amphibolite occur in the *mélange*. While the high metamorphic temperatures needed to produce garnet amphibolite from its basalt protolith seem anomalous to a subduction zone setting, the presence of blueschist facies rocks in

the mélangé matrix, which can only be formed under the high-pressure, low-temperature conditions of subduction zones, confirms a subduction history. Many of the isolated garnet-amphibolite blocks are encircled by mineralogical rinds. Several of the amphibolite blocks and rinds were collected and studied in an attempt to determine the metamorphic history of the material. Although coherent rock units provide a means to study metamorphic history of materials within a clearer tectonic and structural context, exotic blocks provide a case study for the use of isolated products of a high-temperature reaction without a bedrock context to determine reaction conditions, origin, and mechanism. Isolated blocks of garnet-amphibolite encircled by mineralogical rinds were studied in an attempt to determine information about the physical, hydrothermal fluid, and metamorphic history of the material.

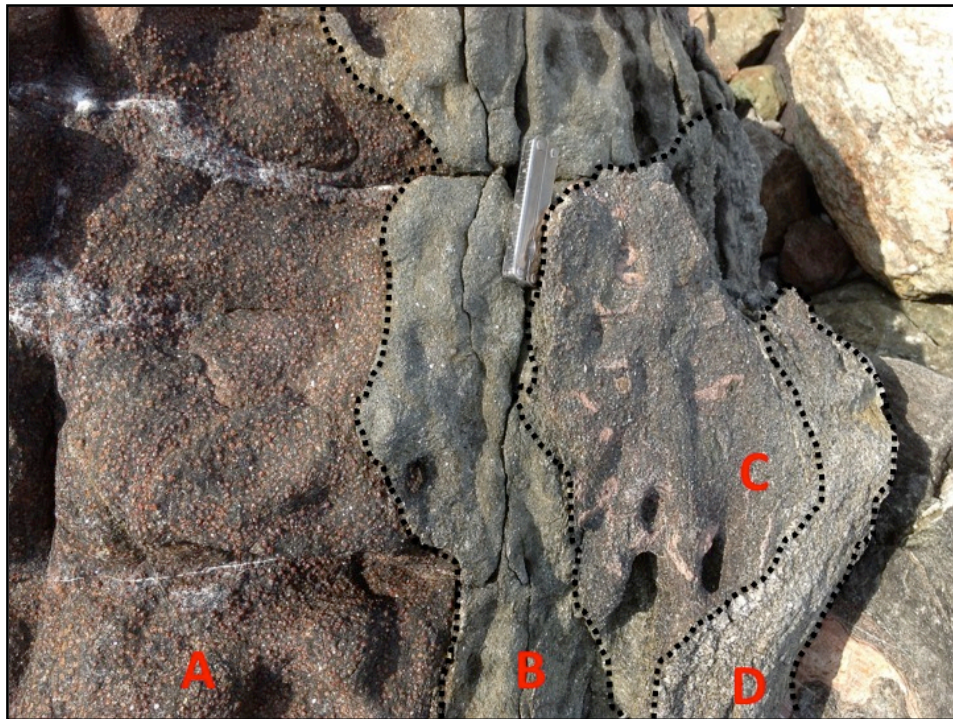


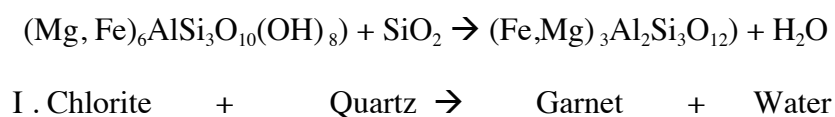
Figure 3. Sample RIP1 rind layers around garnet-amphibolite block. Material A is block (garnet-amphibolite), material B is a primary rind layer, material C is a distinct secondary rind layer, and material D is a distinct third rind layer. Layer B encircles the block completely, remnants of layer C and D occur on one side of the block.

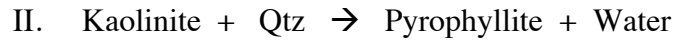
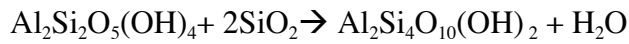
Subduction Zones

Subduction zones are convergent plate boundaries that can form between continental tectonic plates and oceanic tectonic plates. The denser oceanic plate sinks into the mantle beneath the continental plate due to buoyancy, where the oceanic plate material is exposed to higher temperatures and pressures. Material is then uplifted back to the surface as more oceanic plate is fed into the system (Foster, 1988). The product found on the Earth's surface is a *mélange* or mixture of mechanically crushed material (called matrix) surrounding some remaining larger and intact, often circular in nature, rock units (blocks) (Grove et al. 2008).

Subduction zone environments juxtapose materials with disparate chemical compositions such as basaltic ocean crust, sediment from the accretionary wedge that accumulates adjacent to the continent, and ultramafic (low-Si) rocks of the mantle. These materials are subjected to high pressures and elevated temperatures that generate hydrous fluids through compression and geochemical reactions that produce metamorphic rocks (Bebout, 2012). The hydrothermal fluids released by metamorphic reactions have the ability to react with minerals in the subduction zone, partially dissolving minerals and transporting elements by fluid flow. Through the action of these fluids, some elements may be redistributed among subduction zone rocks, changing their chemical compositions (Penniston-Dorland, 2011).

Devolatilization Reaction Examples:





Metamorphism and Facies

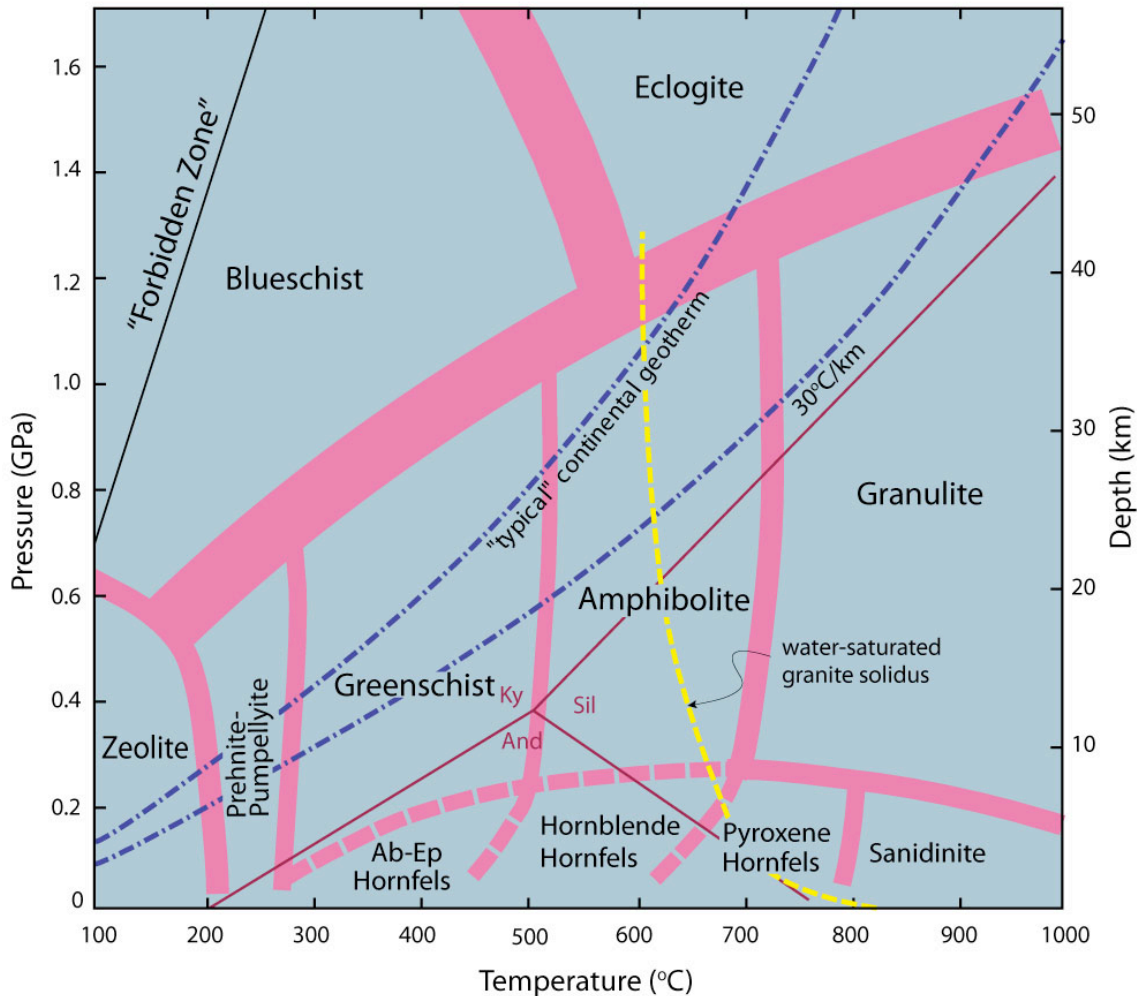


Figure 4. Diagram showing pressure and temperatures for various facies of meta-basaltic (metamorphosed oceanic crust) rocks. Facies are general mineral assemblages that are thermodynamically stable for a given bulk composition (whole-rock chemistry) at a specific temperature and pressure. From Winter 2010; Brown and Mussett 1993.

Sediment and rocks are made of collections of minerals, which are crystalline solids. These solid phases will react with one another to achieve chemical equilibrium if enough energy is available, e.g. if the temperature is high enough. There can be a pore

fluid present (principally water) that will help the reactions occur, but because of the low porosity of most rocks, many reactions take place in the solid state. Equilibrium in this context is on a local scale (e.g., minerals in contact) because of the difficulty of movement of atoms in a densely-packed crystalline lattice. Through study of metamorphic rocks, laboratory experiments at high pressure, and thermodynamic calculations, geologists know what the equilibrium mineral assemblages (facies) should be at the temperatures and pressures of metamorphism.

Indeed, metamorphism reactions of oceanic crust basalt, which is an extrusive, dark-colored, fine-grained igneous rock composed principally of clinopyroxene $(Ca,Na)(Mg,Fe)(Si_2O_6)$ and plagioclase feldspar $(Na,Ca)(Si,Al)_4O_8$, have been studied so that known mineral assemblages occur in specific temperature-pressure groups. Figure 4 above shows the names of these groups, called facies, according to reaction conditions.

This property is guided by the fact that any natural chemical system at equilibrium will manifest itself as a particular assemblage of coexisting phases in accordance with the concepts of thermodynamic equilibria and Gibb's phase rule. Heated rocks therefore aggregate into stable phases of minerals at equilibrium, and changes in such an equilibrium, such as temperature or pressure shifts, shift the phase equilibria and recrystallize the rock through a change of the mineral assemblage (Winter, 2010). These chemical processes due to the addition of heat or pressure on a material are known as metamorphism. A reactant or initial material, called a protolith, will reform and crystallize when exposed to changes in temperature and pressure according to the phase rule (Winter, 2010). It is these phases, characterized by assemblages of minerals, which are divided into the above named facies for meta basaltic rocks.

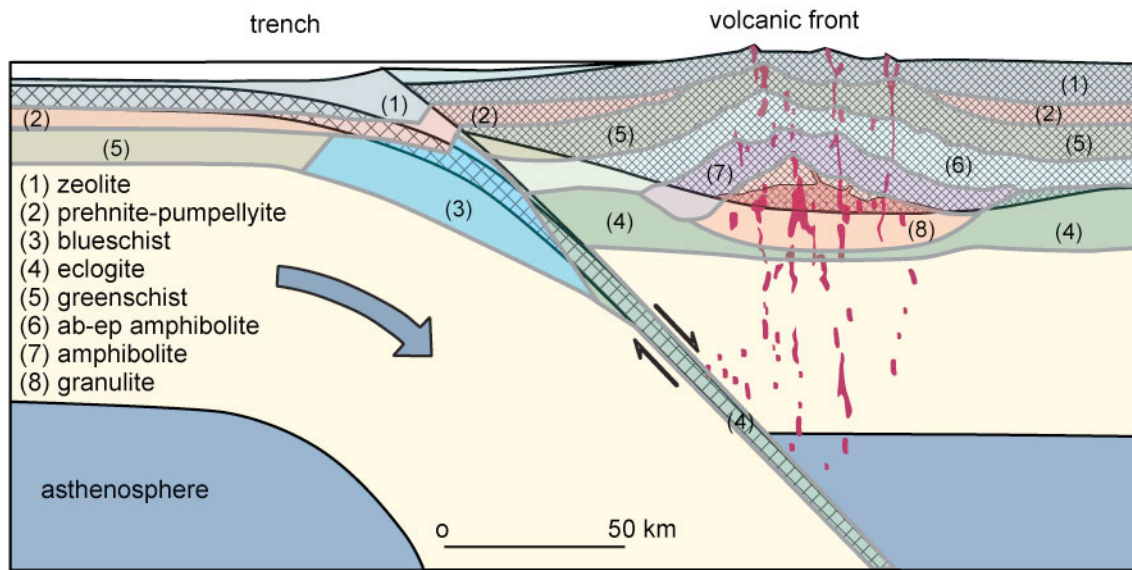


Figure 5. Generalized, observed locations of formation of various facies in an island arc setting. (3) represents the subduction zone accretion that usually forms a mélangé zone of blueschist facies, as theoretically expected on Catalina Island, CA. From Ernst 1976.

Facies have been observed to form at characteristic locations which host the required, associated pressure-temperature conditions. For example, the intense heat and moderate pressure of sub-Earth volcanic systems provide an ideal environment for the formation of higher-grade (higher temperature) facies such as amphibolite and granulite facies rocks. Nearby, with slightly higher pressures but lowered temperatures, eclogite-facies have been observed to originate (see Fig. 5).

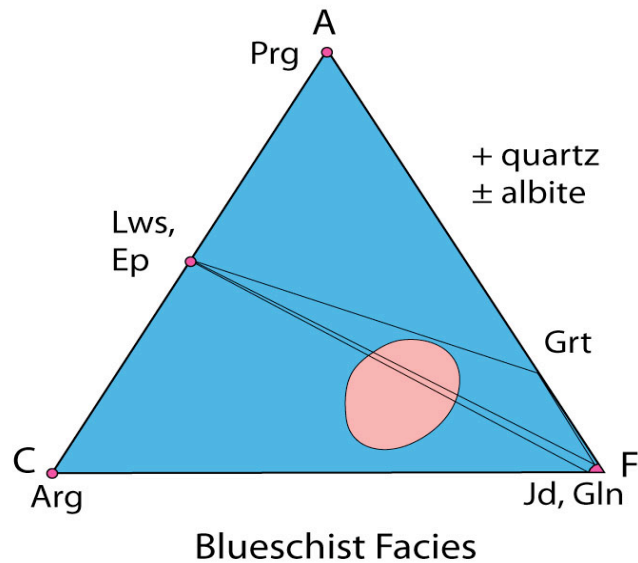


Figure 6. Triangular diagram showing the aluminum (A), calcium (C) and iron (F) content of the main phases of the blueschist facies, showing three phases that are stable in equilibrium conditions. Gray lines connect minerals that are in equilibrium. The blueschist facies is characterized by any tertiary combination of the above minerals, where Prg is paragasite, an amphibole group mineral ($\text{NaCa}_2(\text{Mg,Fe})_4\text{Al}(\text{Si}_6\text{Al}_2)\text{O}_{22}(\text{OH})_2$), Lws is lawsonite ($\text{CaAl}_2\text{Si}_2\text{O}_7(\text{OH})_2 \cdot (\text{H}_2\text{O})$), Ep is epidote ($\text{Ca}_2(\text{Al,Fe})_3(\text{SiO}_4)_3(\text{OH})$), Grt is garnet ($(\text{Ca,Mg,Fe,Mn})_3\text{Al}_2(\text{SO}_4)_3$), Jd is jadeite ($\text{NaAlSi}_2\text{O}_6$), Gln is glaucophane ($[\text{Na}_2(\text{Mg}_3\text{Al}_2)\text{Si}_8\text{O}_{22}(\text{OH})_2]$), and Arg is aragonite (CaCO_3 , pseudomorph of calcite). From Winter 2010.

Blueschist is a meta-basaltic rock facies formed only by high pressure and low temperature conditions and characterized by the presence of the blue hydrous mineral glaucophane ($[\text{Na}_2(\text{Mg}_3\text{Al}_2)\text{Si}_8\text{O}_{22}(\text{OH})_2]$), an amphibole group mineral. Some samples of blueschist, including those on Catalina Island, contain a hydrous calcium aluminum sorosilicate mineral called lawsonite ($\text{CaAl}_2\text{Si}_2\text{O}_7(\text{OH})_2 \cdot (\text{H}_2\text{O})$), which is indicative of moderate pressure and low temperature reactions (see Fig. 6)(Nesse, 2009; Winter, 2010).

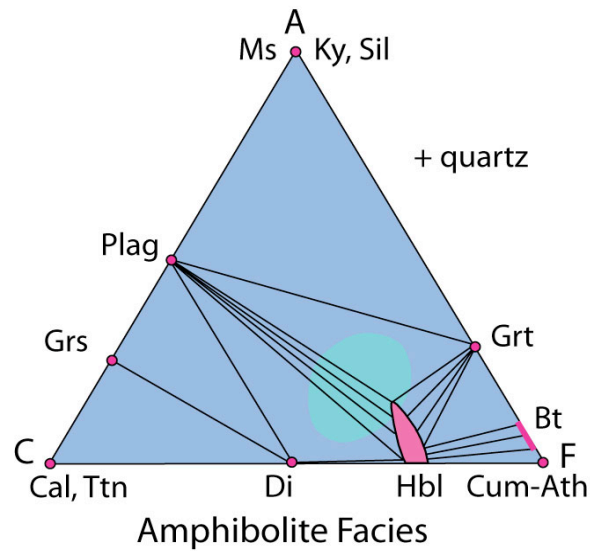


Figure 7. Triangular diagram showing the aluminum (A), calcium (C) and iron (F) content of the main phases of the amphibolite facies, showing three phases that are stable in equilibrium conditions. Gray lines connect minerals that are in equilibrium. The amphibolite facies is characterized by any tertiary combination of the above minerals, where Ms is muscovite ($\text{KAl}_2(\text{AlSi}_3\text{O}_{10})(\text{OH})_2$), Ky is kyanite (Al_2SiO_5), Sil is sillimanite (Al_2SiO_5 , pseudomorph of kyanite), Plag is plagioclase ($(\text{Na,Ca})(\text{Si,Al})_4\text{O}_8$), Grt is garnet ($(\text{Mg,Fe,Mn})_3\text{Al}_2(\text{SO}_4)_3$), Bt is biotite ($\text{K}(\text{Mg,Fe})_3\text{AlSi}_3\text{O}_{10}(\text{OH})_2$), Grs is grossular garnet ($\text{Ca}_3\text{Al}_2(\text{SO}_4)_3$), Cum-Ath is a solid solution between amphibole-group minerals cummingtonite ($[\text{Mg}_7\text{Si}_8\text{O}_{22}(\text{OH})_2]$) and anthophyllite ($(\text{Mg, Fe})_7\text{Si}_8\text{O}_{22}(\text{OH})_2$), Hbl is hornblende ($(\text{Ca,Na})_2 3(\text{Mg,Fe,Al})_5(\text{Al,Si})_8\text{O}_{22}$), Di is pyroxene-group mineral diopside ($\text{MgCaSi}_2\text{O}_6$), Cal is calcite (CaCO_3), and Ttn is titanite (CaTiSiO_5). From Winter 2010.

The amphibolite facies is characterized by higher temperatures and a typical equilibrium mineral assemblage or paragenesis of hornblende ($(\text{Ca,Na})_2 3(\text{Mg,Fe,Al})_5(\text{Al,Si})_8\text{O}_{22}$), plagioclase ($(\text{Na,Ca})(\text{Si,Al})_4\text{O}_8$), and garnet ($(\text{Ca,Mg,Fe,Mn})_3\text{Al}_2(\text{SO}_4)_3$) (see Fig. 7).

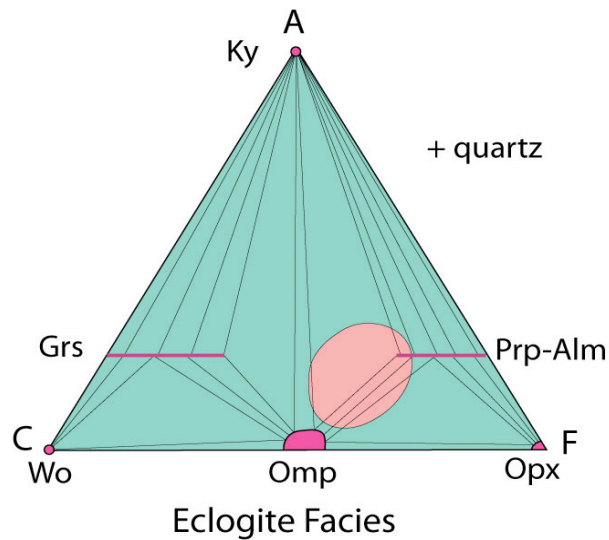


Figure 8. Triangular diagram showing the aluminum (A), calcium (C) and iron (F) content of the main phases of the eclogite facies, showing three phases that are stable in equilibrium conditions. Gray lines connect minerals that are in equilibrium. The eclogite facies is characterized by any tertiary combination of the above minerals, where Ky is kyanite (Al_2SiO_5), Grs is grossular garnet ($\text{Ca}_3\text{Al}_2(\text{SO}_4)_3$), Prp-Alm is a solid solution between garnet end-members pyrope ($\text{Mg}_3\text{Al}_2(\text{SO}_4)_3$) and almandine ($\text{Fe}_3\text{Al}_2(\text{SO}_4)_3$), Wo is wollastonite (CaSiO_3), Omp is clinopyroxene mineral omphacite ($((\text{Ca},\text{Na})(\text{Mg},\text{Fe},\text{Al})\text{Si}_2\text{O}_6)$), and Opx is orthopyroxene ($((\text{Mg},\text{Fe},\text{Ca})(\text{Mg},\text{Fe},\text{Al})(\text{Si},\text{Al})_2\text{O}_6)$). From Winter 2010.

The eclogite facies is characterized by lower temperatures than the amphibolite facies and an equilibrium assemblage of minerals such as omphacite (clinopyroxene)

$((\text{Ca},\text{Na})(\text{Mg},\text{Fe},\text{Al})\text{Si}_2\text{O}_6)$, garnet ($((\text{Ca},\text{Mg},\text{Fe},\text{Mn})_3\text{Al}_2(\text{SO}_4)_3)$), or orthopyroxene

$((\text{Mg},\text{Fe},\text{Ca})(\text{Mg},\text{Fe},\text{Al})(\text{Si},\text{Al})_2\text{O}_6)$ (Fig. 8).

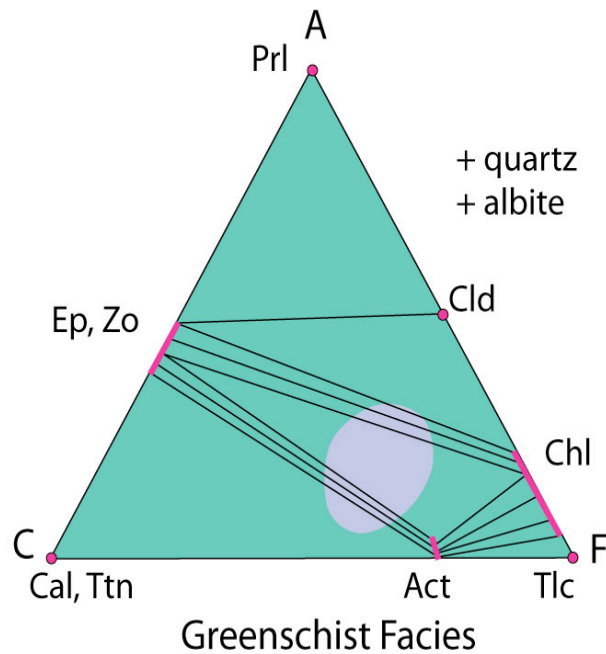


Figure 9. Triangular diagram showing the aluminum (A), calcium (C) and iron (F) content of the main phases of the greenschist facies, showing three phases that are stable in equilibrium conditions. Gray lines connect minerals that are in equilibrium. The greenschist facies is characterized by any tertiary combination of the above minerals, where Prl is pyrophyllite, Cld is chloritoid ($(\text{Fe,Mg,Mn})_2\text{Al}_4\text{Si}_2\text{O}_{10}(\text{OH})$), Ep, Zo are epidote ($\text{Ca}_2(\text{Al,Fe})_3(\text{SiO}_4)_3(\text{OH})$) and zoisite ($\text{Ca}_2\text{Al}_3(\text{SiO}_4)_3(\text{OH})$), Chl is chlorite ($(\text{Mg,Fe,Li})_6\text{AlSi}_3\text{O}_{10}(\text{OH})_8$), Tlc is talc ($\text{Mg}_3\text{Si}_4\text{O}_{10}(\text{OH})_2$), Act is actinolite ($\text{Ca}_2(\text{Mg,Fe})_5\text{Si}_8\text{O}_{22}(\text{OH})_{22}$), Cal is calcite (CaCO_3), and Ttn is titanite (CaTiSiO_5). Albite ($\text{NaAlSi}_3\text{O}_8$) and quartz (SiO_2) are present as needed to balance the system. From Winter 2010.

The greenschist facies is characterized by lower temperatures and pressures than the eclogite facies and an equilibrium assemblage of minerals such as chlorite

$(\text{Mg,Fe,Li})_6\text{AlSi}_3\text{O}_{10}(\text{OH})_8$, albite ($\text{NaAlSi}_3\text{O}_8$), and talc ($\text{Mg}_3\text{Si}_4\text{O}_{10}(\text{OH})_2$) (Fig. 9).

A combination of the above-described facies are present on Catalina Island, California (Fig. 10). The island has been described as a subduction zone, which are areas of high pressure and relatively lower temperature metamorphism. These environments characteristically form rocks of the blueschist facies. While the high temperatures needed to produce garnet amphibolite seem anomalous to a subduction zone setting, the presence of blueschist facies rocks in the mélangé matrix, which can only be formed under such

high-pressure, low-temperature conditions of subduction zones, confirms a subduction history. Despite this, isolated blocks of garnet amphibolite occur in the mélange. Other facies of meta-basaltic rocks present on Catalina Island include greenschist and eclogite (Platt, 1975).

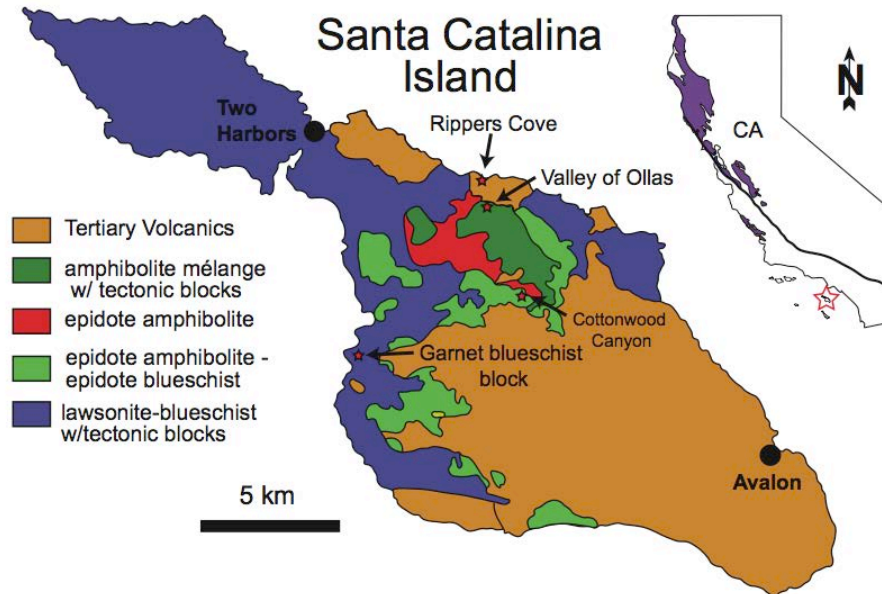


Figure 10. Geologic map of Catalina Island. Catalina Island, California is characterized by a variety of facies of metamorphic rocks as well as areas of igneous materials. The lowest facies present is lawsonite-blueschist followed by epidote blueschist, epidote amphibolite, and amphibolite. Tertiary volcanics are igneous beds dated back to the Tertiary period (65 to 2.6 million years ago) (Foster, 1988).

Previous Work on the Catalina Schist and the Amphibolite Blocks

Previous studies of the metamorphic histories of different parts of the Catalina Schist have shown that the high grade amphibolites formed 122-115 Ma at ~8-11kbar and ~640-750°C, with lower grade formations of epidote blueschist forming at ~8kbar, 450°C and lawsonite-blueschist forming at ~9kbar, 300°C (Grove et al., 2008; Sorensen and

Barton, 1987; Platt, 1975). All facies appear to have formed at comparatively similar pressures but at a variety of temperatures.

J. P. Platt proposed in 1975 that the additional heat needed to form amphibolite facies materials found in the Catalina subduction complex was supplied by an underthrust hanging wall. As the subduction zone pulled in cold ocean floor, the hanging wall decreased in temperature and the sediments in the accretionary wedge were exposed to lower temperatures of metamorphism. This produced progressively lower grades of material over time. This explanation was widely accepted until 2008 when Grove et al. proposed that such a subduction zone would still have been colder than required to form amphibolites facies rocks (Grove et al., 2008). The study instead proposed that in this subduction system, the high temperatures required to form amphibolites was supplied by forearc basin compression (Fig. 11). Parts of this hot, compressed material underthrust the magmatic arc of the Peninsular Ranges batholith and remained in the thrust close enough to the batholith to receive the heat necessary to form amphibolite rocks (Grove et al., 2008). The lowest grade materials, the lawsonite-blueschist and lawsonite-albite formations, formed much later in thermal conditions consistent with a subduction zone setting (Grove et al., 2008). They were then accreted on top of the rest of the Catalina complex as more material was fed into the subduction zone system through movement of the tectonic plates and were later exposed due to erosion. (Grove et al., 2008)

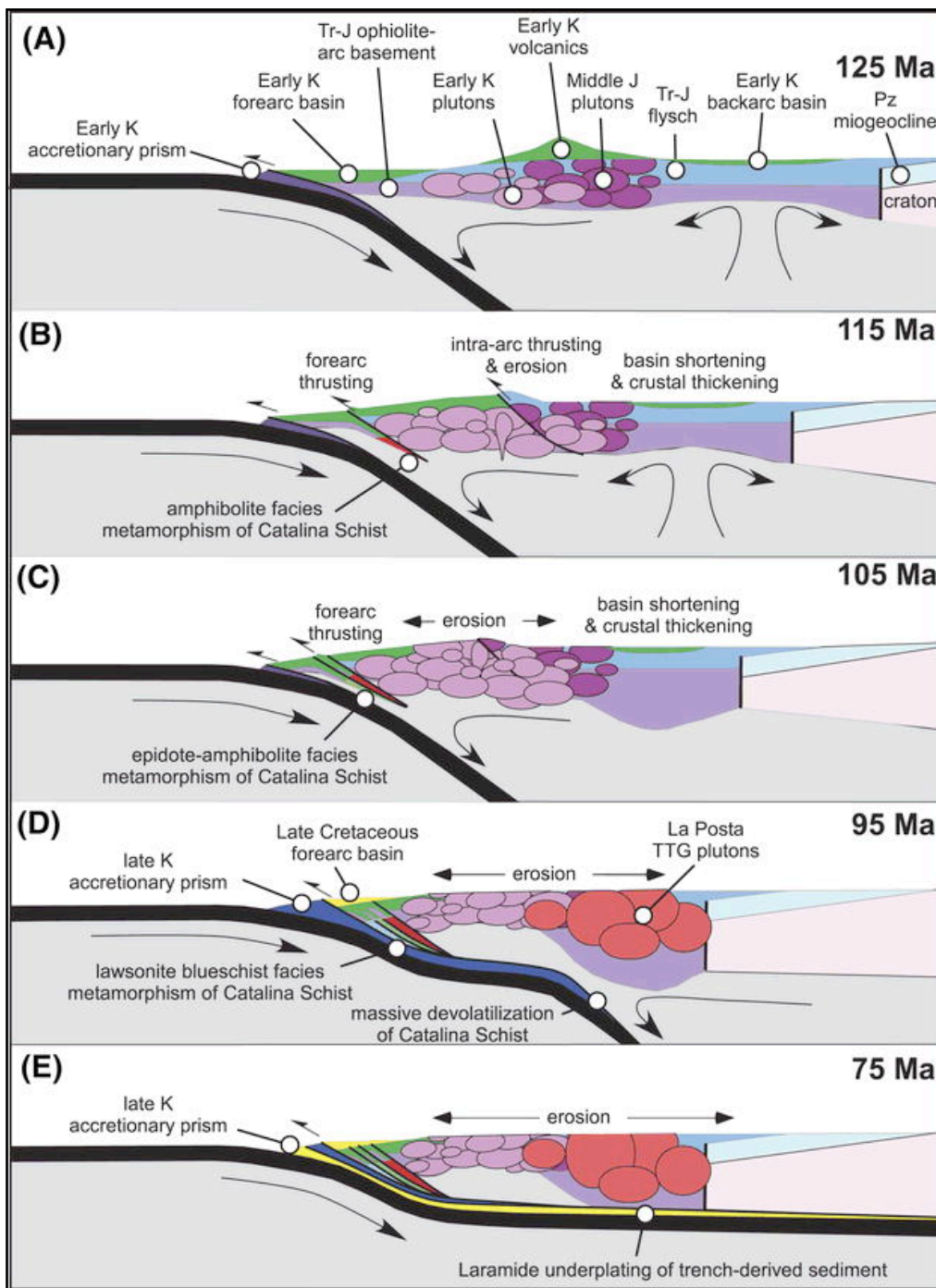


Figure 11. Subduction zone system of Catalina Island, California over time illustrating mechanism for extra heat to form garnet-amphibolite facies, adapted from Grove 2008. In (A), a normal subduction zone system is present. The forearc basin is not compressed and the temperature-pressure conditions are that of any other subduction zone. Material is beginning to pile up at the accretionary wedge. In (B), the forearc underthrust has begun, as has inter-arc erosion exposing some of the basaltic oceanic crust to amphibolite-facies temperatures. In (C), progressively cooler facies of meta-basalts have begun to form. (D) shows the location of the formation of blueschist facies rocks in the Catalina subduction complex. (E) shows how erosion has revealed each layer on the island, which is how the Catalina Schist formation can be observed today.

One way to enrich the current understanding of the tectonic history of Catalina Island is to take a closer look at such garnet-amphibolite blocks, some of which are distinctively encircled by mineralogical rinds, and ask what unique system and materials could have formed such a product. Penniston-Dorland et al. proposed in a 2011 abstract that an early episode of mechanical mixing between mafic block and mélangé materials allowed for the formation of such rind materials. They state that garnet growth in both block and rind materials occurred after mechanical mixing, and that fluid infiltration caused alteration of garnet to chlorite and the growth of white micas. These conclusions were drawn from rind trace element concentrations of Cr, Ni, Zr, Al₂O₃, TiO₂, FeO, which reflect mobility of elements in the system during later tectonic stage fluid infiltration, at the time of great physical mixing of the system (Penniston-Dorland et al. 2011). Penniston-Dorland et al. describe a single primary rind layer on the garnet-amphibole blocks and performed trace-element analyses on the samples. Conversely, this study observed multiple layers of concentric rinds with unique textures and assemblages in each layer, and examined bulk and major element chemistry rather than trace element chemistry.

The matrix material of Catalina Island is compositionally equivalent serpentinite (Sorensen, 1989), an ultra-mafic rock formed from mantle material that is typically high in magnesium, iron, nickel, and chromium (Winter, 2010). Sorensen's 1989 x-ray fluorescence analyses of the bulk compositions of both the serpentinite matrix and garnet-amphibolite blocks reveal key differences in concentrations of aluminum, iron, magnesium, and calcium between these two materials introduced in the subduction complex (Table 1; Fig. 12).

	Serpentinite Matrix	Block
SiO₂	39.2	38.8
TiO₂	0.09	5.5
Al₂O₃	0.8	16.1
FeO	8.1	19.3
MnO	0.12	0.46
MgO	35.9	8.3
CaO	0.29	7.1
Na₂O	0.03	0.82
K₂O	0.08	0.19
H₂O	13.6	0.5

Table 1. Bulk compositions of serpentinite matrix sample from Catalina Island, CA and garnet-amphibolite block encircled in rind from Sorensen 1989 obtained from X-ray fluorescence experiments.

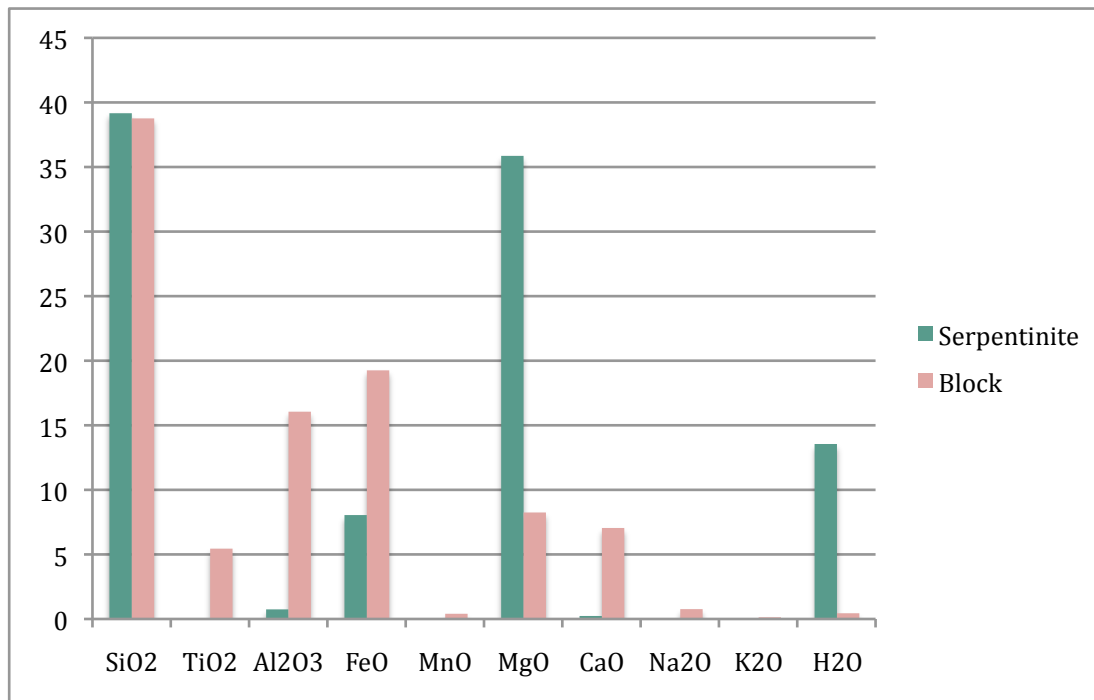


Figure 12. Comparative bulk compositions of serpentinite matrix sample from Catalina Island, CA and garnet-amphibolite block encircled in rind from Sorensen 1989 obtained from X-ray fluorescence experiments.

Concentrations of aluminum, iron, and calcium are all greater in the bulk composition of the block, while magnesium and water are both much greater in the bulk composition of the matrix. The two largest differences in the two materials are the high

concentrations of water and magnesium in the serpentinite. While the physical conditions of a subduction zone create an opportunity for mechanical mixing, this chemical disparity creates an opportunity for chemical reactions to occur (Table 1; Fig. 12)

Objectives of this Study

This study sought to determine why there are mineralogical rinds on Catalina Island amphibolite blocks. Are the rind layers the result of a chemical reaction with the mélange zone matrix and subsequent chemical diffusion? Are they the result of the physical process of mechanical mixing during uplift as proposed by Penniston-Dorland et al., 2011? To what extent were fluids involved in this process, and did fluids introduce new materials to the reaction (as proposed by Sorenson and Bebout, 1987; Bebout and Barton, 1989)? To answer these questions, this study focused on three coarse-grained blocks of garnet-amphibolite from Ripper's Cove, Catalina Island. The samples were divided by material into core and one or more concentric rinds. Two of the three samples exhibited garnets in both the core and rind materials.

Fluids and Metasomatism

Fluids are believed to be present almost ubiquitously during metamorphic reactions within the Earth, such as in subduction zone environments. Indeed, devolatilization reactions are strongly exothermic and therefore favorable and abundant in metamorphic reaction environments (Winter, 2010). However, there is often little to no direct remaining evidence concerning their nature in the rocks that are collected at the Earth's surface, as virtually all fluid once in equilibrium with the mineral assemblage during metamorphism was released from the material during tectonic uplift as pressure on

the system decreased. While fluid inclusions in crystals may give evidence of the chemical composition of fluids present in the system, they do not give evidence regarding the quantity of fluid present during the reaction (Winter 2010).

However, understanding the role of fluids in a system is an important component of understanding the equilibrium conditions and chemical changes of the system during metamorphism, called metasomatism. Fluids are able to dissolve material, transport solutes, precipitate minerals, exchange chemical components as they react with minerals, and catalyze deformation processes by weakening rocks (Winter 2010). To understand the extent to which fluid has modified the metamorphic system, certain clues must be carefully examined such as veins, indicative of fluid transport paths, and hydrated minerals (e.g. chlorite, epidote, which are water-enriched versions of garnet and plagioclase minerals).

All units of the Catalina Schist, from blueschist to amphibolite facies metasedimentary, metamafic and meta-ultramafic rocks, show veining and alteration that reflect fluid transport and metasomatism during prograde (increasing temperature/pressure) metamorphism and uplift. Examples of such alteration includes water-rich minerals (chlorite, epidote), fluid inclusions in crystals such as garnets (Sorenson, 1987) and quartz, and textural hydration such as small cross-cutting veins. Veins are remnants of fluid paths that moved through the rock and indicate the passage of fluid through a system. Bebout's 1989 isotopic studies of the metasomatic events of the Catalina Schist found that the likely source of metasomatic fluids is lower temperature, devolatilization reaction fluids from other, sediment-rich parts of the subduction zone. Though he does not discuss block and rind textures, it can be inferred that such fluid processes could have been present during the production or chemical modification of

rinds on amphibolite blocks. Data on garnet fluid inclusions in the blocks of these rocks has been examined by Sorenson (1987), which proved to be water-rich.

Mechanical Mixing

In this study, mechanical mixing can be described as a physical blending of materials. This mixing is not controlled by the chemical properties of components of the material.

Diffusion Reactions of Solids

Diffusion is the process by which components move through a medium. Diffusion through a crystalline solid is called lattice diffusion and is driven by chemical potential gradients (Winter 2010). Classical experiments in solid-state chemical diffusion consisted of bringing together two solid materials of uniform but different composition across a planar interface. The temperature was raised, and interdiffusion occurred in the direction normal to the interface. After a lapse of time, a concentration-penetration curve could be determined along the diffusion direction. The results of such experiments were interpreted through the application of Fick's 1st and 2nd laws of diffusion in solids, which for one-dimensional diffusion are as follows:

$$\text{I } J = -D(\partial c/\partial x)$$

$$\text{II } (\partial c/\partial t) = \partial(D\partial c/\partial x)/\partial x$$

where J is flux (atoms/cm²sec), C is concentration (atoms/cm³), and D is the diffusion coefficient, also known as diffusivity (cm²sec⁻¹) (Bube et al., 1954). Fick's laws relate the flux of material across a given plane as proportional to the concentration gradient across the plane (Bube, 1954; Winter, 2010).

These mathematical models approximate diffusion as the result of a concentration gradient, $\partial C/\partial x$. The substances will have a natural tendency to decrease the gradient by moving in a direction that will disperse atoms more evenly. Diffusive flux increases with temperature and steepness of the concentration gradient. Given enough time, this flow of impurities will result in homogeneity between two materials, causing the net flow of atoms to stop (Bube et al., 1954). This will lower the free energy of the whole system (Winter, 2010).

While diffusion is more effective in a fluid-rich, porous environment, intergranular diffusion may occur in dense solids such as metamorphosed basalts. Atom transfer by diffusion to form rinds is likely to take place along grain boundaries between crystals rather than through crystal lattices themselves. As ordered crystal lattices form, “leftover” atoms that could not fit into the structure sit outside of the grain boundaries in a disordered assemblage. Water often ends up outside of the crystal and piles up in this pathway (Brady, 1977; Dohmen and Milke, 2010) These boundaries are where exchanges between atoms usually begin at high or low temperatures. More porous substances, with higher diffusivity constants, will alter more readily. Mélange materials, which do not have the tight, crystalline, mosaic formation of rocks and is more porous, allows for nearly free fluid-flow.

Amphibole Structure

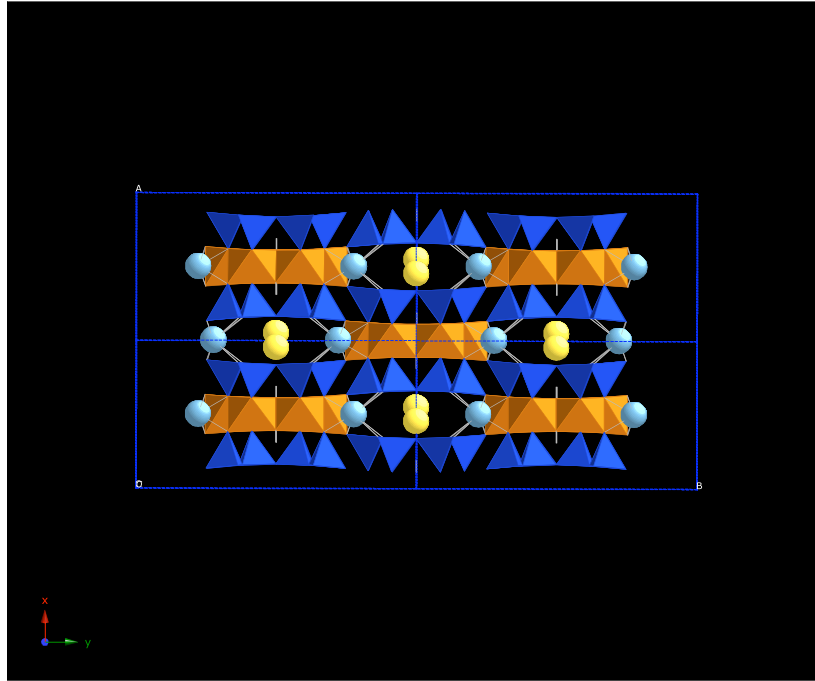


Figure 13. Amphibole geometric structural model. Octahedral sites (orange) usually contain 2+ cations (Fe, Mg, Mn), and sometimes Al, coordinated with oxygen, tetrahedral sites (blue) contain Si or Al coordinated with oxygen, M4 sites (blue) contain Ca or Na (larger cations), and A sites (yellow) may be vacant or contain Na, K if there is excess. Made with CrystalMaker software.

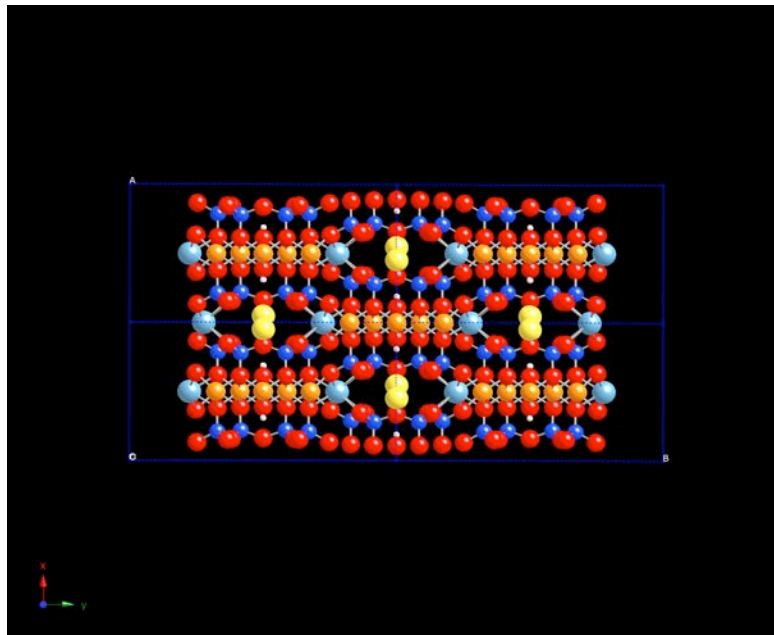


Figure 14. “Ball and stick” model of amphibole structure. Red balls are oxygen, blue are Si, orange are Fe, Mg, Mn or Al, large, light blue are large cations such as Ca or Na, yellow is the A-site (vacant or Na, K). Made with CrystalMaker software.

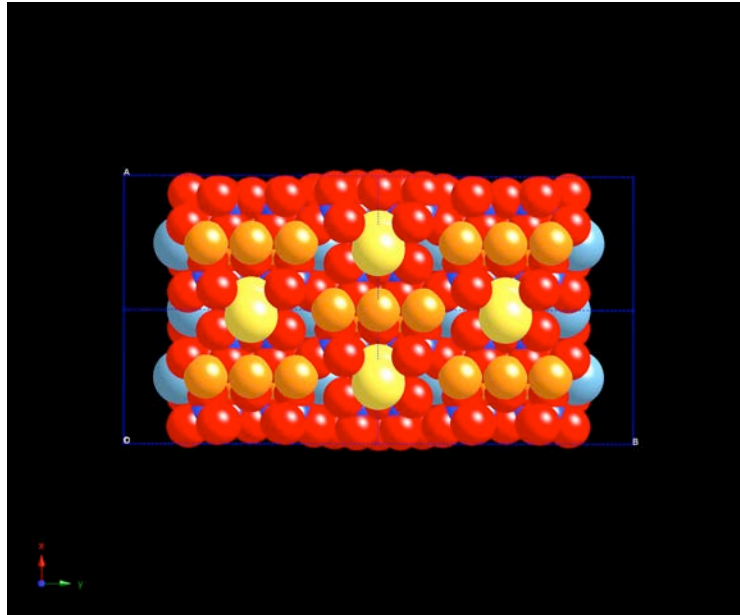


Fig 15. “Space-filled” amphibole model showing relative atomic sizes throughout the crystal structure. Red are oxygen, orange are 2+ cations or aluminum, blue are large cations, dark blue are Si, yellow is the A-site (vacant or Na, K) Open spaces in the structure facilitate diffusion. Made with CrystalMaker software.

Amphiboles are a common group of hydrous minerals found in both metamorphic and igneous rocks. While amphiboles are ubiquitous, and quantifying the diffusion behavior of cations and anions is important in applications of geochronology and geothermometry, relatively little data for diffusion of these minerals exist. This may be due to the fact that maintaining stability of hydroxyl-bearing phases is difficult under a broad range of experimental conditions (Cherniak, 2010). Because of their comparatively open structure, filled with small vacancies (Fig. 15), amphiboles are relatively porous, permeable crystals and therefore more susceptible to chemical diffusion than more densely-packed minerals.

Garnet Structure

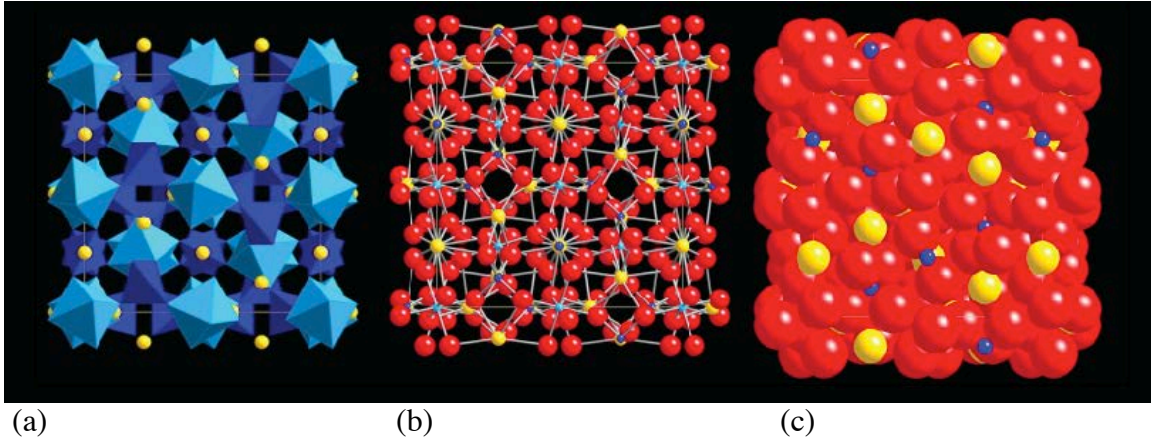


Figure 16. Garnet structures (a) Geometric model, where light blue octahedral sites contain Al; dark-blue tetrahedrons contain Si and oxygen, and yellow sites represent Ca, Mg, Fe, Mn,. (b) “Ball and stick” model where red is oxygen, yellow is Si, light blue is Al, and dark-blue are 2+ cations (c) “Space-filled” model showing relative atomic sizes throughout the crystal lattice and how densely packed garnet crystals are. Red is oxygen, yellow is Si, light blue is Al, and dark-blue are 2+ cations. Made with CrystalMaker software.

Garnets are common metamorphic minerals indicative of high temperature reactions. The garnet group is described by the crystal-chemical formula $X_3Y_2[ZO_4]_3$, where $X = Ca^{2+}, Mg^{2+}, Fe^{2+}, Mn^{2+}$ etc., $Y = Al^{3+}, Fe^{3+}, Cr^{3+}, Ti^{4+}, Mn^{3+}, V^{3+}, Zr^{3+}$ etc. and $Z = Si^{4+}$ (also Al^{3+}, Fe^{3+} or substitution of $[ZO_4]$ by $[OH]_4$). The most common end-members, and those used in this study, are grossular ($Ca_3Al_2(SiO_4)_3$), almandine ($Fe_3Al_2(SiO_4)_3$), spessartine ($Mn_3Al_2(SiO_4)_3$), and pyrope ($Mg_3Al_2(SiO_4)_3$) (Nesse, 2009). Combinations of these end-members are found in nature in varying concentrations and arrangements.

The densely packed structure of garnets (Fig. 16 (C)) allows for little permeability (Winter, 2010), though grain-boundary diffusion may alter the rim composition of garnets especially at high temperatures. This low rate of diffusion in garnet prevents its composition from changing at low temperatures. However, the higher rate of diffusion in

amphiboles may allow for such a diffusion reaction to occur in low-temperature conditions.

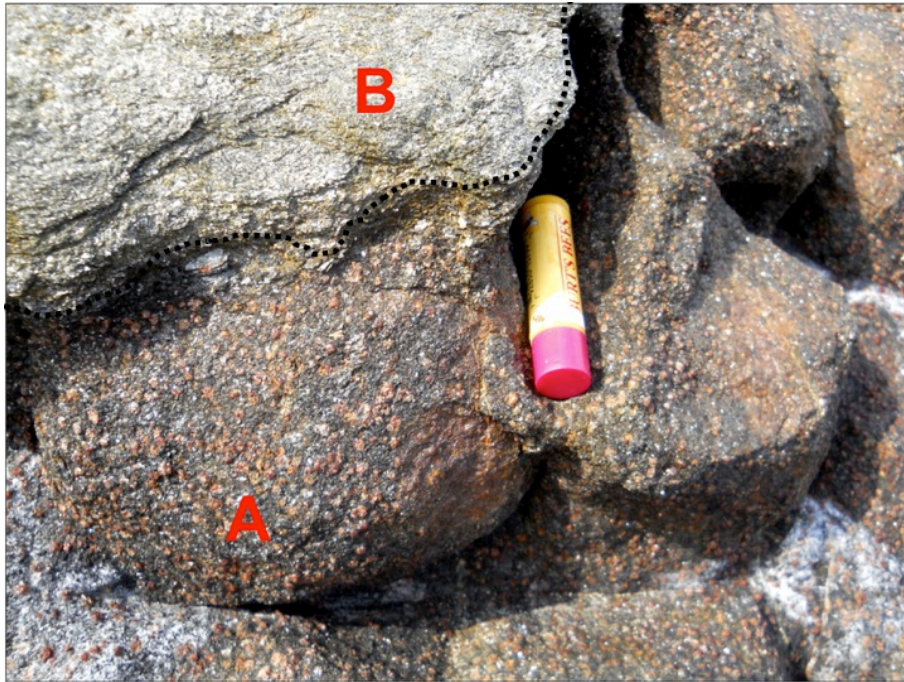


Figure 17: Garnet-amphibolite block (chapstick) and rind layer B (top of photograph) on sample RIP1

Methods



Figure 18. Sample RIP1 in the field.

Field methods

Over 25 samples were collected from Ripper's Cove, Santa Catalina Island during two visits to the location in July, 2012 using rock hammers and chisels. Samples were bagged and mailed to Oberlin College for processing in August. This study focused on samples from three blocks.



Figure 19. Tools and hand samples in the field at Ripper's Cove, Catalina Island, CA.

Optical light microscopy

Samples were cut and polished into thin sections at Oberlin College with supervision and assistance from specialist laboratory technician. Thin sections were examined via optical light microscopy using petrographic microscope techniques to obtain mineral assemblage and textural information. Each thin section is composed of only one block or rind material.

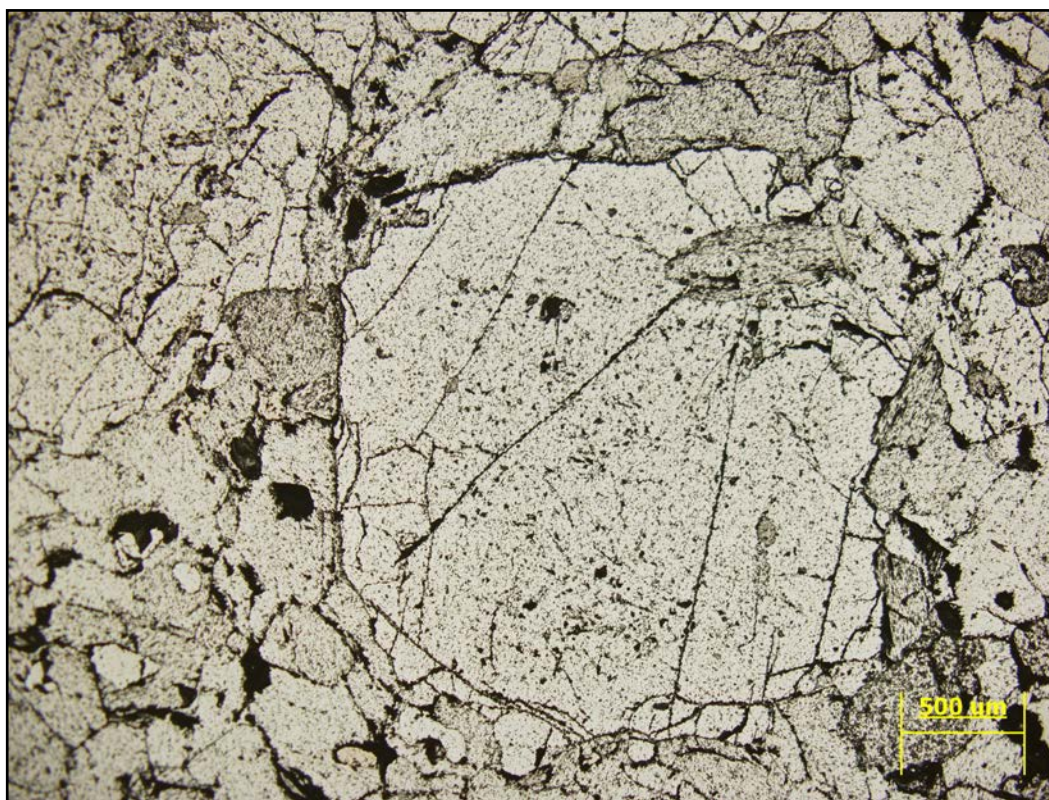


Figure 20. Photomicrograph of sample RIP4A showing a large garnet in plane polarized light.

Scanning Electron Microscopy (SEM) and Energy-Dispersive X-Ray Spectroscopy (EDS)

Selected carbon-coated thin sections were examined using scanning electron microscopy to identify crystal grains of interest. The FEI Quanta 400 SEM was standardized using mineral standards analyses in conjunction with the RZAF procedure of standardization. Analyses were collected at 20 kV with a 2.5 nA beam current. EDAX TEAM (Texture and Elemental Analytical Microscopy) and EDAX GENESIS software packages were used to confirm mineral assemblage as well as to collect and quantify major element chemistry analyses for garnets and amphiboles.

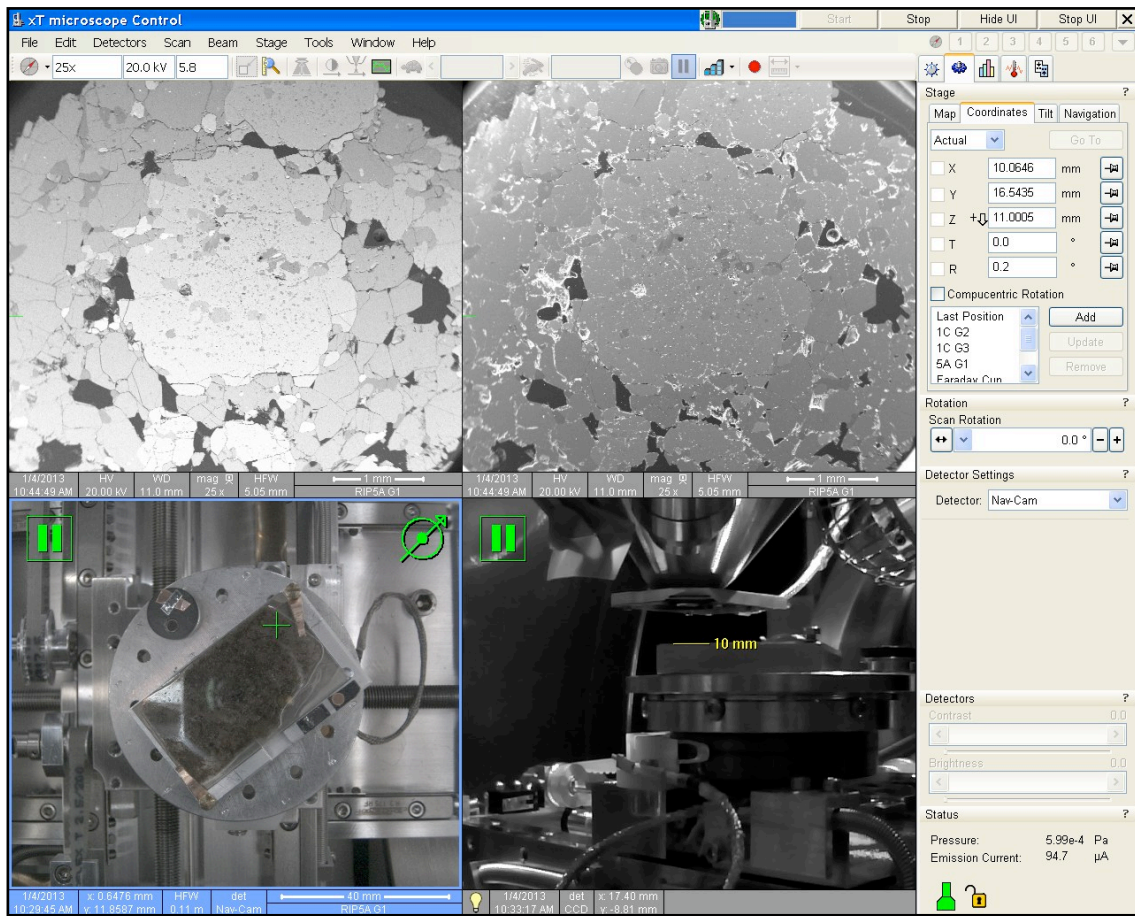


Figure 21. Screen capture of Scanning Electron Microscope display (top right image) and Electron Dispersive Spectroscopy display (top left image) focused on a large garnet in sample RIP1A (thin section view from top in bottom left image, mounted thin section view inside of microscope vacuum chamber in bottom right image).

Thermometry

Geothermometers use mathematical relationships to relate chemical composition equilibria with temperature formation conditions. Such an equation (Fig. 22) relating iron and magnesium in equilibrated garnet and hornblende mineral pairs was applied to samples from this study.

$$T (^{\circ}\text{C}) = \frac{1504 + 1784(X_{\text{Ca}}^{\text{Grt}} + X_{\text{Mn}}^{\text{Grt}})}{\ln K_{\text{D}(\text{Fe}^{2+}/\text{Mg})}^{\text{Grt-Hbl}} + 0.720} - 273$$

where

$$K_{\text{D}(\text{Fe}^{2+}/\text{Mg})}^{\text{Grt-Hbl}} = \frac{(\text{Fe}^{2+}/\text{Mg})^{\text{Grt}}}{(\text{Fe}^{2+}/\text{Mg})_{\text{M1-M3}}^{\text{Hbl}}}$$

$$X_{\text{Ca}}^{\text{Grt}} = \frac{\text{Ca}}{\text{Ca} + \text{Mn} + \text{Fe}^{2+} + \text{Mg}} \text{ in garnet}$$

$$X_{\text{Mn}}^{\text{Grt}} = \frac{\text{Mn}}{\text{Ca} + \text{Mn} + \text{Fe}^{2+} + \text{Mg}} \text{ in garnet}$$

Figure 22. Garnet-Hornblende thermometer equation from Ravenna 2000.

This thermometer was calibrated using combined data sets both from experiments where garnet and hornblende were equilibrated under known temperature-pressure conditions and from garnet and hornblende compositions in natural samples where good estimates of temperature-pressure conditions were obtained from other geothermometers (Ravna 2000).

Results

Sample descriptions

RIP1: Rock sample composed of block + three rinds layers divided into RIP1A, RIP1B, RIP1C and RIP1D.



Fig 23. Sample RIP1, layers of rinds were divided into sections A, B, C, and D according to these physical textures, and thin sections RIP1A, RIP1B, RIP1C and RIP1D were studied.

RIP1A



Figure 24. Sample RIP1A, Garnet-Amphibolite block material. Red crystals are garnets, darker mass of crystals are hornblende amphiboles.



Figure 25. Scan of thin section of sample RIP1A

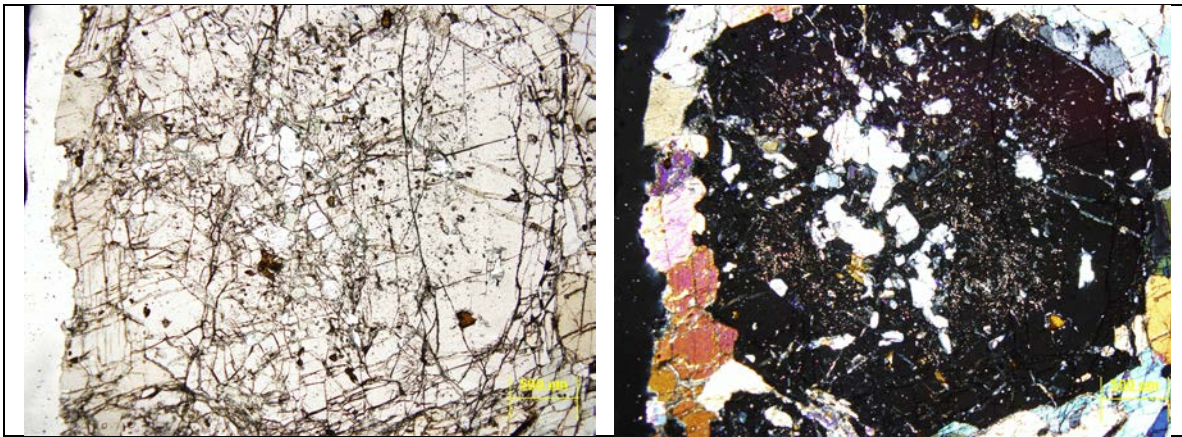


Figure 26. Sample RIP1A under plane-polarized light (left) and crossed polars (right). Focused on garnet with larger inclusions toward the center and powdery inclusions toward the rim. Scale bar at bottom right is 500 μ m.

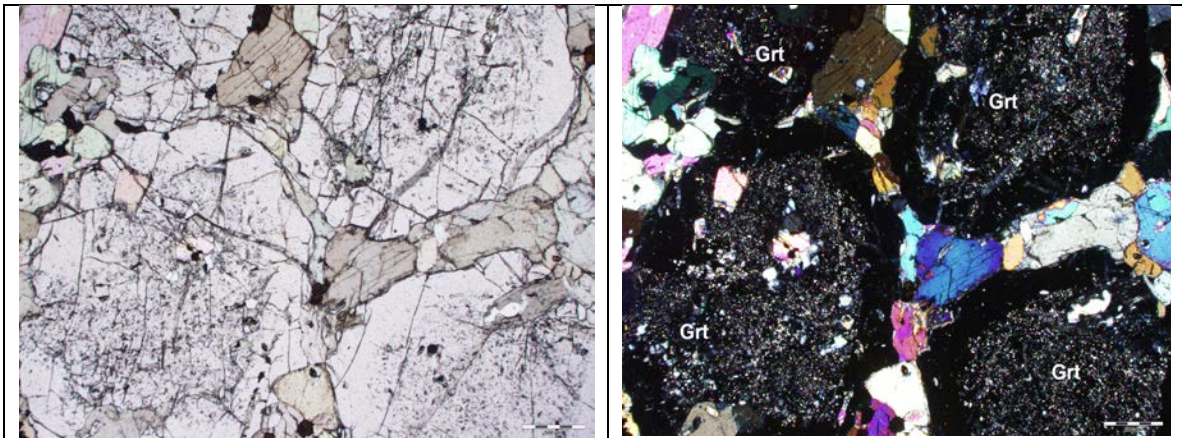


Figure 27. Sample RIP1A under plane-polarized light (left) and crossed polars (right) focused on garnet and hornblende grains. Scale bar at bottom right is 500 μ m.

This sample is composed of garnet-amphibolite block material with a mineral assemblage of garnet ($(\text{Ca,Mg,Fe,Mn})_3\text{Al}_2(\text{SO}_4)_3$) (30%) and hornblende ($(\text{Ca,Na})_2 3(\text{Mg,Fe,Al})_5(\text{Al,Si})_8\text{O}_{22}$) (65%). Garnet size is large, from 1500 to 2000 μ m in diameter. Garnet inclusions include epidote ($\text{Ca}_2(\text{Al,Fe}^{3+})_3\text{Si}_3\text{O}_{12}(\text{OH})$), zoisite ($\text{Ca}_2\text{Al}_3(\text{SiO}_4)_3(\text{OH})$), chlorite ($(\text{Mg,Fe,Li})_6\text{AlSi}_3\text{O}_{10}(\text{OH})_8$), and quartz (SiO_2). Garnet inclusions vary texturally, with larger central inclusion grains at the core surrounded by smaller, powdery-textured

inclusions toward the rim (Fig. 26). Some inclusions are cut texturally by small quartz “veins.” Accessory minerals include rutile (TiO_2) and apatite ($\text{Ca}_5(\text{PO}_4)_3(\text{OH})$).

RIP1B



Fig 28. Sample RIP1B and RIP1A in field. RIP1A is dark in color, touching the rock hammer, and RIP1B is lighter in color in the foreground of the photo.



Figure 29: Scan of thin section of sample RIP1B

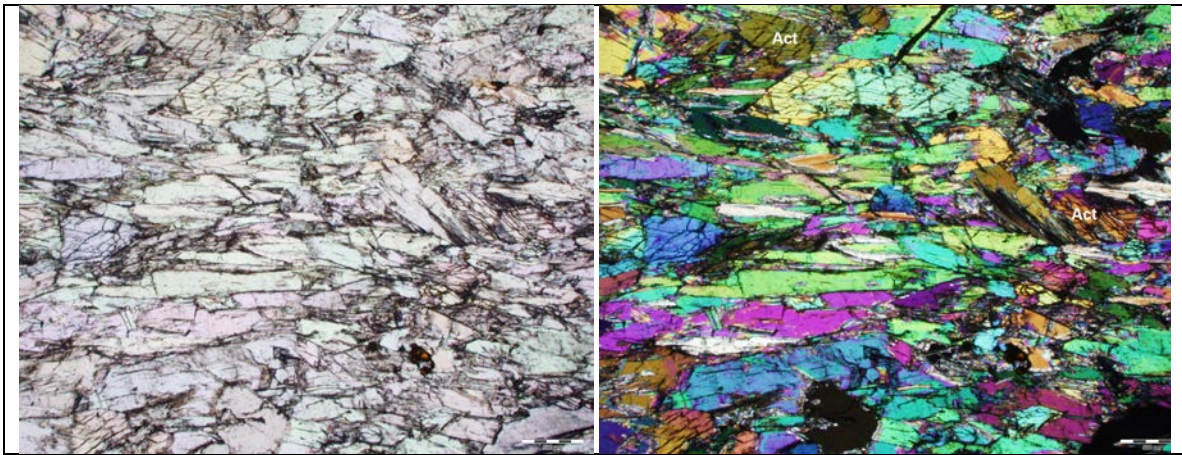


Figure 30. Sample RIP1B under plane-polarized light (left) and crossed polars (right) focused on actinolite grains. Scale bar at bottom right is 500 μ m.

This sample is composed of the first rind layer, occurring between RIP1A and RIP1C. The material is more greenish in color and occurs in a mineral assemblage of chlorite ($(\text{Mg,Fe,Li})_6\text{AlSi}_3\text{O}_{10}(\text{OH})_8$) (30%), phengite ($\text{K}(\text{AlMg})_2(\text{OH})_2(\text{SiAl})_4\text{O}_{10}$) (20%), and actinolite ($\text{Ca}_2(\text{Mg,Fe})_5\text{Si}_8\text{O}_{22}(\text{OH})_{22}$) (50%). No garnets were found in this sample.

Accessory minerals include rutile (TiO_2) and apatite ($\text{Ca}_5(\text{PO}_4)_3$). The thin section is quilt-like in texture, with equal-sized grains of amphibole and mica distributed throughout.

RIP1C



Fig 31. Sample RIP1C in field. Larger garnets surrounded by amphibole toward top of image, smaller garnets embedded in quartz near Chapstick.

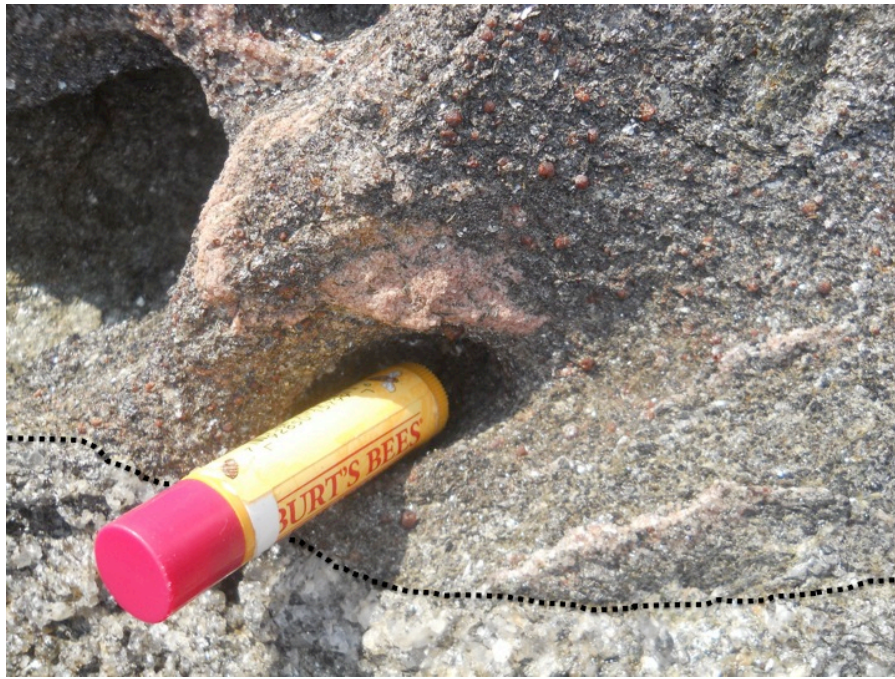


Figure 32. Sample RIP1C in field. Larger garnets surrounded by amphibole toward top of image, smaller garnets embedded in quartz near Chapstick. RIP1D layer meets C layer at the bottom of the photo.



Figure 33: Scan of thin section of sample RIP1C

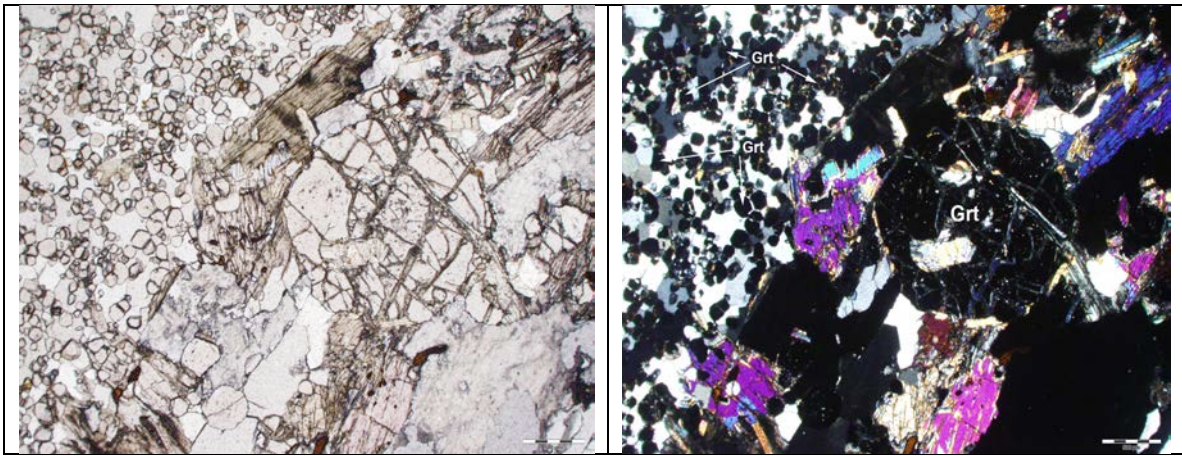


Figure 34. Sample RIP1C under plane-polarized light (left) and crossed polars (right) focused on large and small garnet grains. Scale bar at bottom right is 500 μ m.

This sample is composed of the secondary rind layer, distinct from RIP1B or RIP1D. The mineral assemblage is garnet ((Ca,Mg,Fe,Mn)₃Al₂(SO₄)₃) (30%), chlorite ((Mg,Fe,Li)₆AlSi₃O₁₀(OH)₈) (15%), hornblende ((Ca,Na)₂3(Mg,Fe,Al)₅(Al,Si)₈O₂₂) (35%), phengite (K(AlMg)₂(OH)₂(SiAl)₄O₁₀) (15%), quartz (SiO₂) (5%). Phengite crystals grow around chlorite. Two different sizes of garnets with similar chemical composition are found in this sample (Fig. 3). Smaller garnets are approximately 500 μ m in diameter, larger garnets range from 1500 to 2000 μ m. Smaller garnets are surrounded by quartz, focused on boundaries between quartz crystal grains, and contain few to no inclusions. Larger garnets contain inclusions of quartz (SiO₂), zoisite ((Ca₂Al₃(SiO₄)₃(OH)), and epidote (Ca₂(Al,Fe)₃(SiO₄)₃(OH)). Accessory minerals include rutile (TiO₂) and apatite (Ca₅(PO₄)₃).

RIP1D



Figure 35: Scan of thin section of sample RIP1D

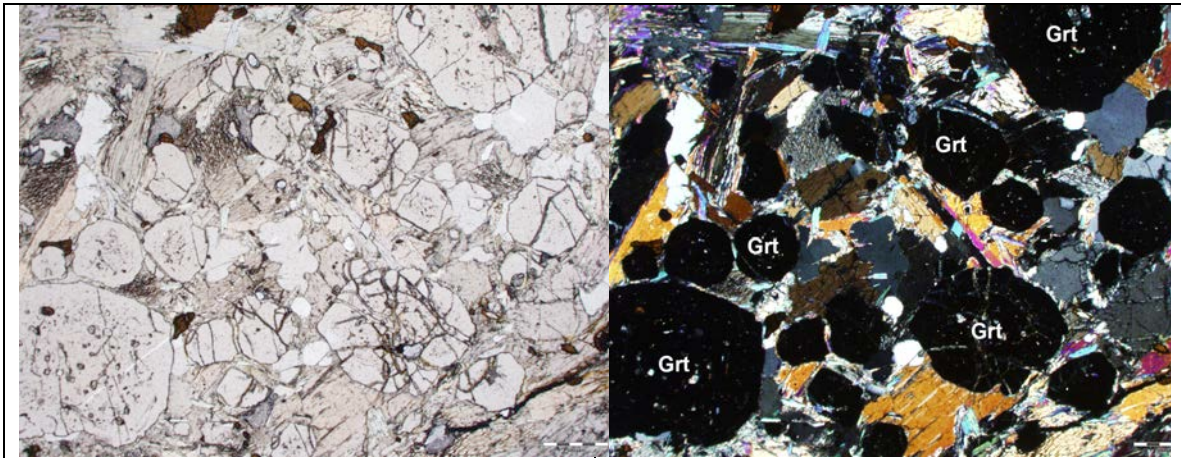


Figure 36. Sample RIP1D under plane-polarized light (left) and crossed polars (right) focused on garnet and quartz grains. Scale bar at bottom right is 500 μ m.

This sample is the tertiary rind layer to garnet-amphibolite block material RIP1A. The mineral assemblage includes garnet ($(\text{Ca},\text{Mg},\text{Fe},\text{Mn})_3\text{Al}_2(\text{SO}_4)_3$) (20%), chlorite $(\text{Mg},\text{Fe},\text{Li})_6\text{AlSi}_3\text{O}_{10}(\text{OH})_8$ (20%), actinolite $(\text{Ca}_2(\text{Mg},\text{Fe})_5\text{Si}_8\text{O}_{22}(\text{OH})_{22})$ (35%), quartz

(25%). Garnets are replaced by chlorite and are approximately 1500µm in diameter.

Accessory minerals include rutile (TiO₂) and apatite (Ca₅(PO₄)₃).

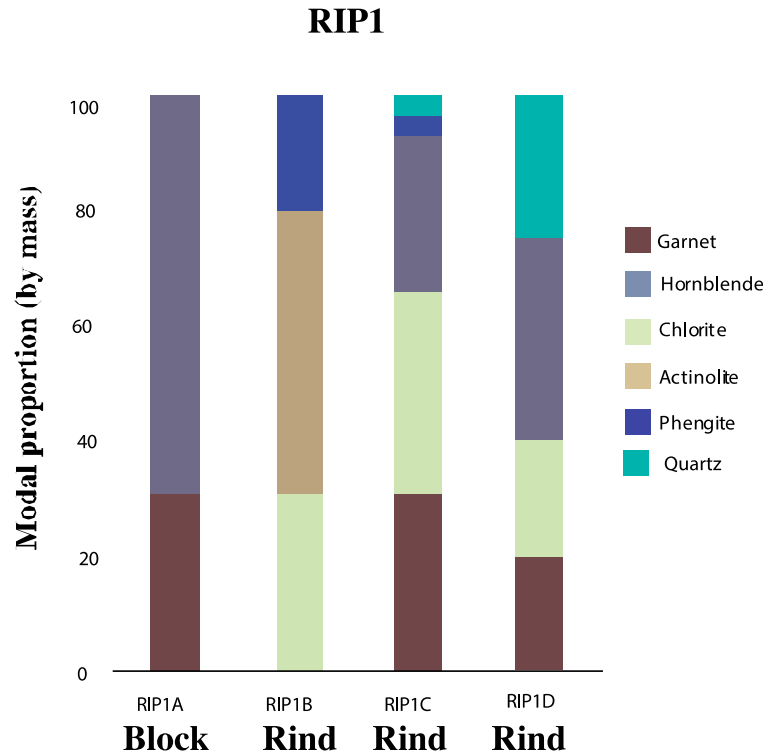


Figure 37: Figure comparing mineral assemblages of different layers of sample RIP1. Mineral assemblages arranged by mode. The core is composed of garnet ((Ca,Mg,Fe,Mn)₃Al₂(SO₄)₃) and amphibolite (hornblende, ((Ca,Na)₂3(Mg,Fe,Al)₅(Al,Si)₈O₂₂)) and the first rind layer is composed of chlorite ((Mg,Fe,Li)₆AlSi₃O₁₀(OH)₈), actinolite amphibole (Ca₂(Mg,Fe)₅Si₈O₂₂(OH)₂₂), and phengite mica (K(AlMg)₂(OH)₂(SiAl)₄O₁₀). RIP1C contains garnets, chlorite, hornblende amphibole, phengite and quartz (SiO₂), and RIP1D contains garnet, chlorite, hornblende, and quartz.

RIP4: Rock sample composed of block + two rind layers divided into samples RIP4A, RIP4B, and RIP4C

RIP4A



Figure 38: Scan of thin section of sample RIP4A

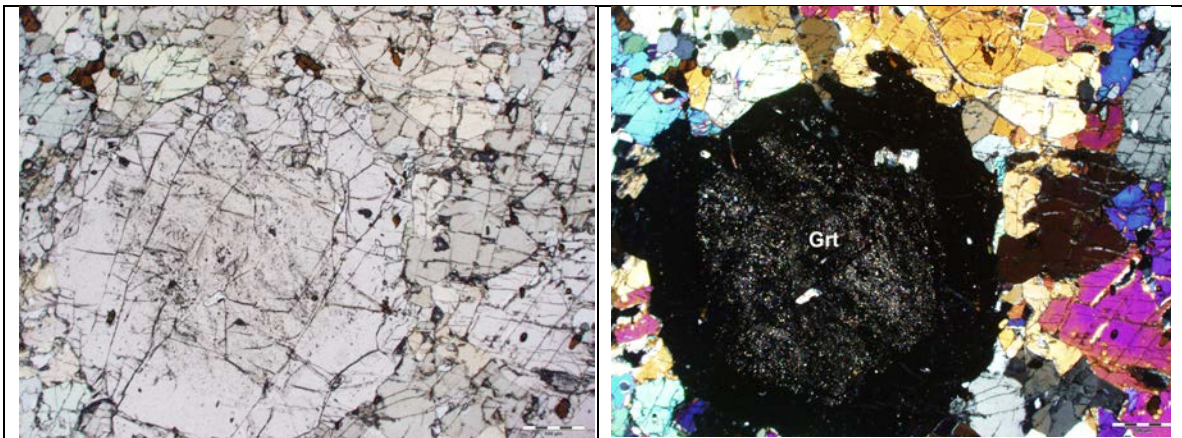


Figure 39. Sample RIP4A under plane-polarized light (left) and crossed polars (right) focused on garnet and hornblende grains. Scale bar at bottom right is 500 μ m.

This sample is composed of garnet-amphibolite block material containing the mineral assemblage of garnet ($(\text{Ca,Mg,Fe,Mn})_3\text{Al}_2(\text{SO}_4)_3$) (35%), chlorite ($(\text{Mg,Fe,Li})_6\text{AlSi}_3\text{O}_{10}(\text{OH})_8$) (10%) and hornblende ($(\text{Ca,Na})_2\text{3}(\text{Mg,Fe,Al})_5(\text{Al,Si})_8\text{O}_{22}$) (55%). Garnet size is large, from 2000 to 2500 μ m in diameter. Garnet inclusions are also

generally large and include epidote ($\text{Ca}_2(\text{Al,Fe})_3(\text{SiO}_4)_3(\text{OH})$), chlorite, and quartz. Garnet inclusions vary texturally, with larger central inclusion grains at the core surrounded by powdery inclusions toward the rim. Chlorite rims or replaces garnets. Accessory minerals include rutile (TiO_2).

RIP4B



Figure 40: Scan of thin section of sample RIP4B

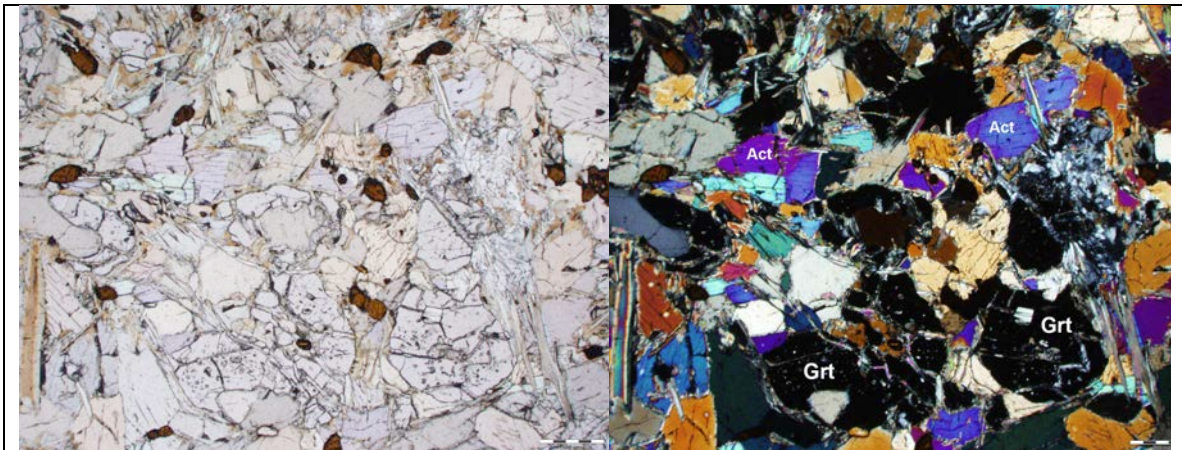


Figure 41. Sample RIP4B under plane-polarized light (left) and crossed polars (right) focused on actinolite and garnet grains. Scale bar at bottom right is 500 μm .

This sample is composed of the first rind layer, located between RIP4A and RIP4C. The amphibole is lighter in color than in RIP4A. The mineral assemblage is chlorite ($(\text{Mg,Fe,Li})_6\text{AlSi}_3\text{O}_{10}(\text{OH})_8$) (20%), garnet ($(\text{Ca,Mg,Fe,Mn})_3\text{Al}_2(\text{SO}_4)_3$) (10%), phengite ($\text{K}(\text{AlMg})_2(\text{OH})_2(\text{SiAl})_4\text{O}_{10}$) (20%), and amphibole (50%). Garnets are highly altered and may be completely surrounded by chlorite. Accessory minerals include rutile (TiO_2) and apatite ($\text{Ca}_5(\text{PO}_4)_3$). The thin section is quilt-like in texture, with equal-sized grains of amphibole and mica distributed throughout.

RIP4C



Figure 42: Scan of thin section of sample RIP4C

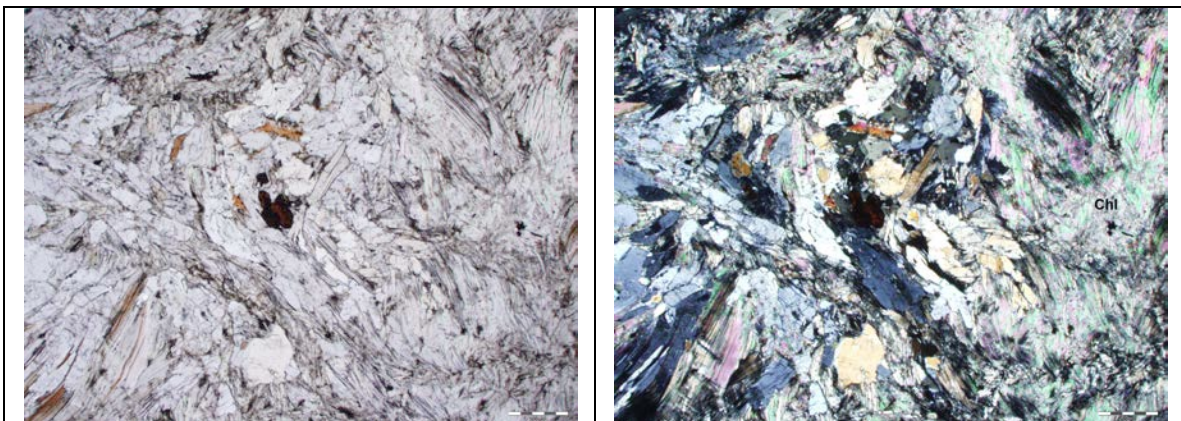


Figure 43. Sample RIP4C under plane-polarized light (left) and crossed polars (right) focused on chlorite and albite grains. Scale bar at bottom right is 500 μm .

This sample is composed of the second rind layer, distinct from RIP4A or RIP4B.

The mineral assemblage is chlorite $((\text{Mg,Fe,Li})_6\text{AlSi}_3\text{O}_{10}(\text{OH})_8)$ (20%), phengite

$(\text{K}(\text{AlMg})_2(\text{OH})_2(\text{SiAl})_4\text{O}_{10})$ (60%), albite $(\text{NaAlSi}_3\text{O}_8)$ (15%) and quartz (SiO_2) (5%).

No garnets were found in this sample. Accessory minerals include rutile (TiO_2) .

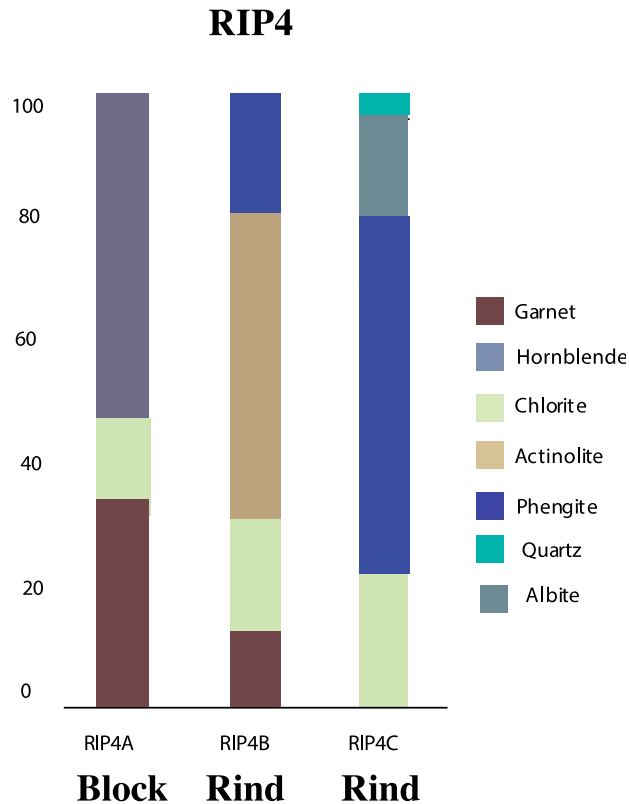


Figure 44: Figure comparing mineral assemblages of different layers of sample RIP4. Mineral assemblages arranged by mode. RIP4A core sample contains mostly garnet $((\text{Ca,Mg,Fe,Mn})_3\text{Al}_2(\text{SO}_4)_3)$, chlorite $((\text{Mg,Fe,Li})_6\text{AlSi}_3\text{O}_{10}(\text{OH})_8)$, and hornblende $((\text{Ca,Na})_2\text{3}(\text{Mg,Fe,Al})_5(\text{Al,Si})_8\text{O}_{22})$. RIP4B sample contains mostly garnet, chlorite, actinolite $(\text{Ca}_2(\text{Mg,Fe})_5\text{Si}_8\text{O}_{22}(\text{OH})_{22})$, and phengite. RIP4C contains mostly chlorite, phengite, albite $(\text{NaAlSi}_3\text{O}_8)$, and quartz (SiO_2) .

RIP5: Rock sample composed of block + one rind layer and divided into samples RIP5A and RIP5B

RIP5A



Figure 45: Scan of thin section of sample RIP5A

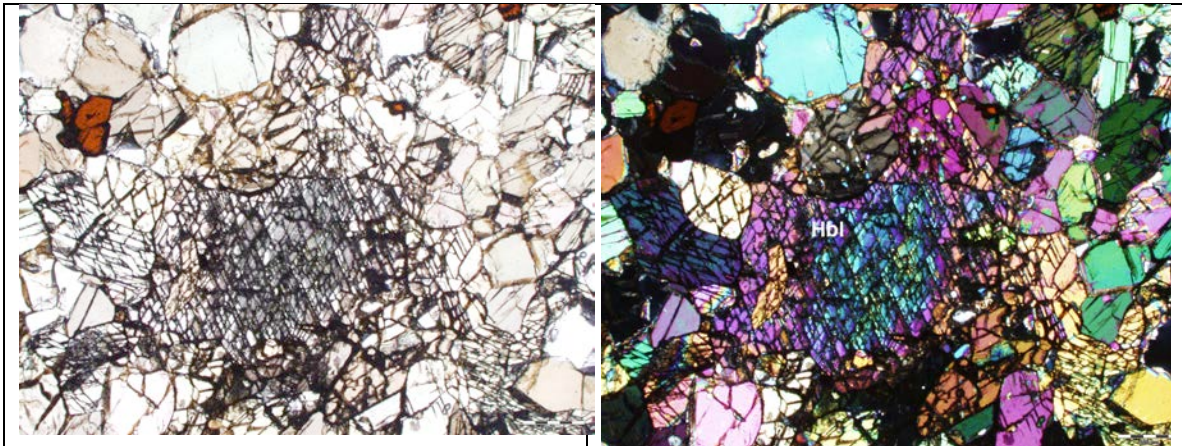


Figure 46. Sample RIP5A under plane-polarized light (left) and crossed polars (right) focused on hornblende grain. Scale bar at bottom right is 500 μ m.

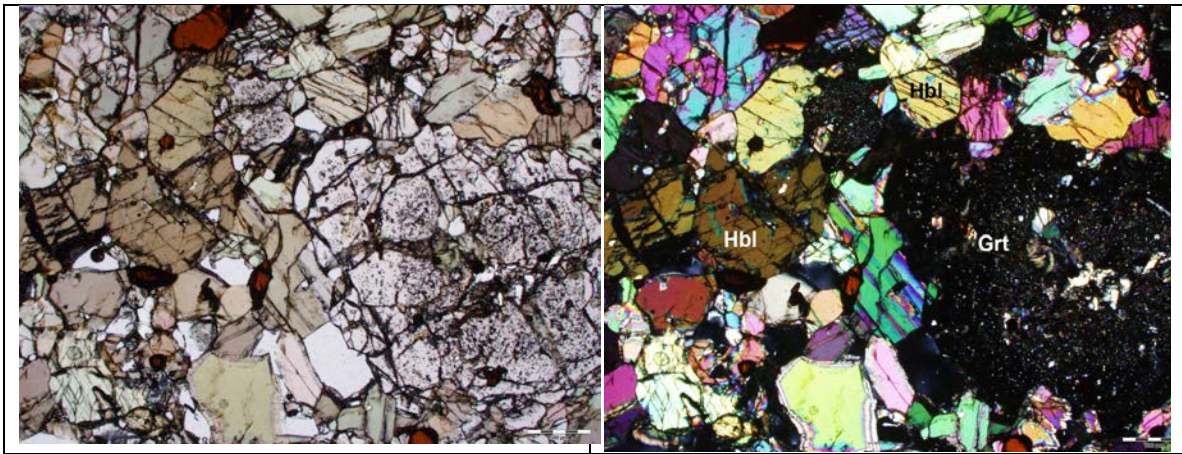


Figure 47. Sample RIP5A under plane-polarized light (left) and crossed polars (right) focused on garnet and hornblende grains. Scale bar at bottom right is 500 μ m.

This sample is composed of garnet-amphibolite block material. The mineral assemblage is garnet ($(Ca,Mg,Fe,Mn)_3Al_2(SO_4)_3$) (35%), phengite ($K(AlMg)_2(OH)_2(SiAl)_4O_{10}$) (10%), hornblende ($(Ca,Na)_2 3(Mg,Fe,Al)_5(Al,Si)_8O_{22}$) (55%), and quartz (SiO_2). Garnet size is large, from 2000 to 2500 μ m in diameter. Garnet inclusions are also generally large and include chlorite ($(Mg,Fe,Li)_6AlSi_3O_{10}(OH)_8$) and quartz (SiO_2). Garnet inclusions vary texturally, with larger central inclusion grains at the core surrounded by powdery inclusions toward the rim. Accessory minerals include rutile (TiO_2) and sphene ($CaTiSiO_5$).

RIP5B



Figure 48: Scan of thin section of sample RIP5B

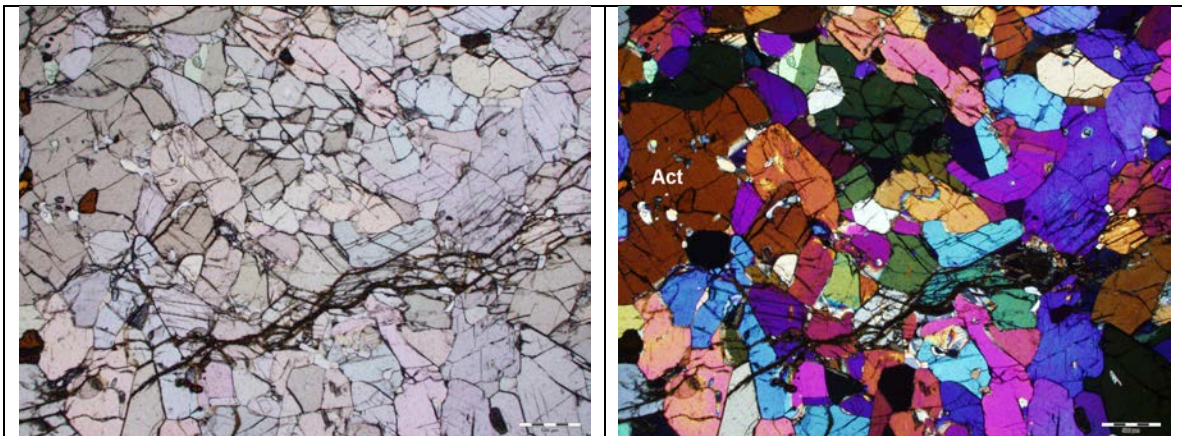


Figure 49. Sample RIP5B under plane-polarized light (left) and crossed polars (right) focused actinolite grains. Scale bar at bottom right is 500 μ m.

This sample is composed of a primary rind layer, surrounding RIP5A. The mineral assemblage is actinolite ($\text{Ca}_2(\text{Mg,Fe})_5\text{Si}_8\text{O}_{22}(\text{OH})_{22}$) (70%) and chlorite ($(\text{Mg,Fe,Li})_6\text{AlSi}_3\text{O}_{10}(\text{OH})_8$) (25%). No garnets were found in this sample. Amphibole

crystals are very uniform in size. Accessory minerals include rutile (TiO_2) and sphene (CaTiSiO_5), including very large sphene crystals (2500 μm in length).

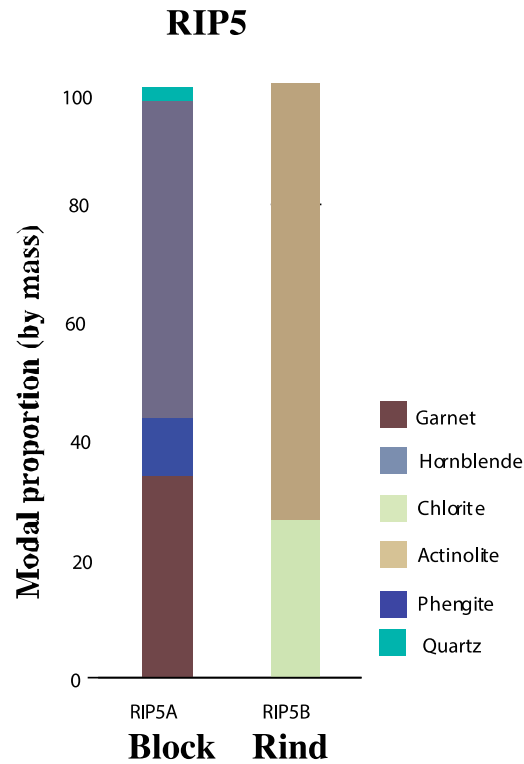


Figure 50: Figure comparing mineral assemblages of different layers of sample RIP5. Mineral assemblages arranged by mode. RIP5A core sample contains mostly garnet ($(\text{Ca},\text{Mg},\text{Fe},\text{Mn})_3\text{Al}_2(\text{SO}_4)_3$), phengite ($\text{K}(\text{AlMg})_2(\text{OH})_2(\text{SiAl})_4\text{O}_{10}$), and hornblende ($(\text{Ca},\text{Na})_2\text{3}(\text{Mg},\text{Fe},\text{Al})_5(\text{Al},\text{Si})_8\text{O}_{22}$). RIP5B is mostly composed of chlorite ($(\text{Mg},\text{Fe},\text{Li})_6\text{AlSi}_3\text{O}_{10}(\text{OH})_8$) and actinolite ($\text{Ca}_2(\text{Mg},\text{Fe})_5\text{Si}_8\text{O}_{22}(\text{OH})_{22}$).

Compositional Chemistry

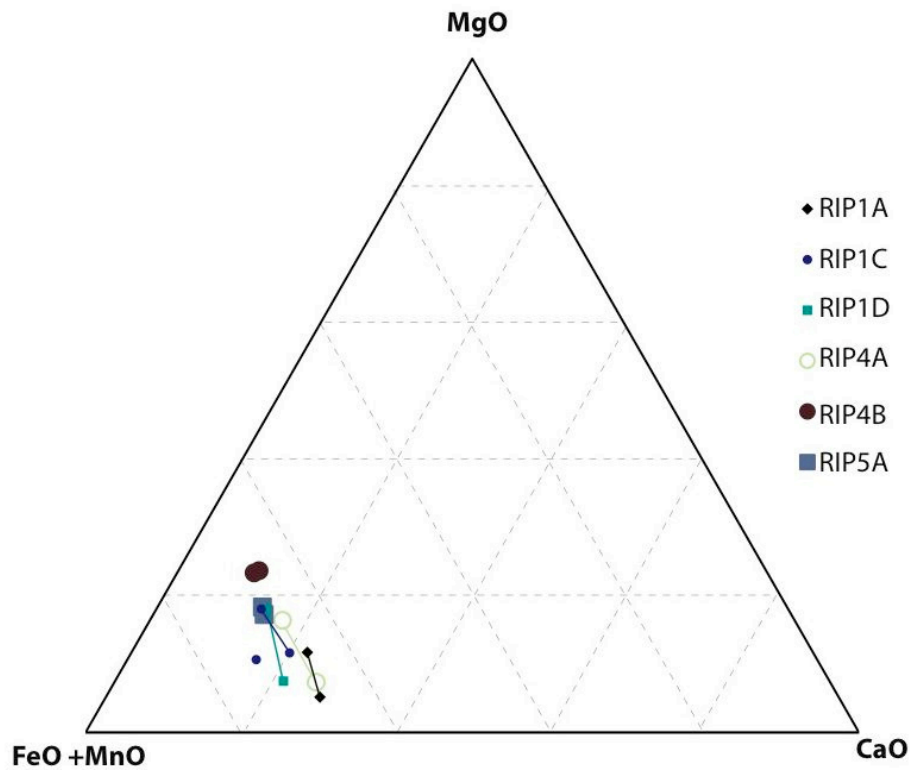


Figure 51. Garnet composition diagram for all garnet-bearing samples in study, examining concentrations of end members ($(\text{Fe,Mn})_3\text{Al}_2(\text{SO}_4)_3$), $\text{Ca}_3\text{Al}_2(\text{SO}_4)_3$, and $(\text{Mg})_3\text{Al}_2(\text{SO}_4)_3$. Data collected using FEI Quanta 400 SEM, quantified using TEAM software and Smith College mineral standards. Lines connect rims and cores of garnet grains, where garnet rims are more calcium-rich and garnet cores are more magnesium-rich.

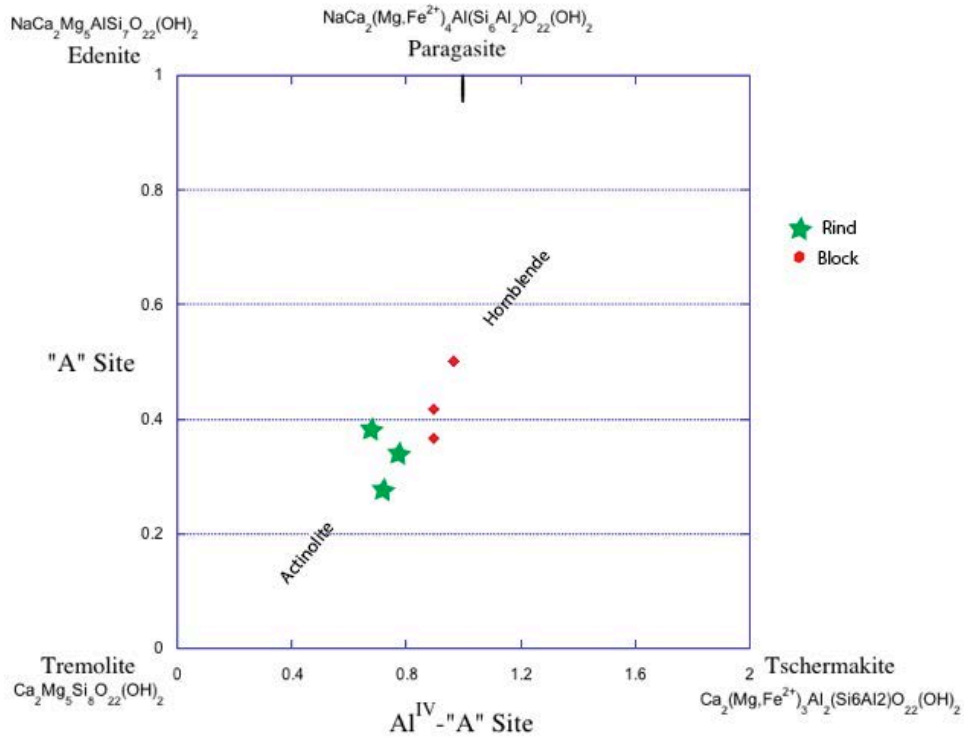


Figure 52. Block and rind amphibole contrasted on the tremolite-edenite-tschermakite end-member system, with the "A" site calculated as occupancy per half unit cell (total number of cations minus 15) and the abscissa calculated as the quantity of tetrahedral aluminum (8.00 minus the number of silicon atoms per half unit cell) minus the calculated A site occupancy.

	RIP1A	RIP1B	RIP1C	RIP1D	RIP4A	RIP4B	RIP4C	RIP5A	RIP5B
SiO₂	44.52	34.63	44.49	40.43	42.78	40.48	45.19	42.47	47.24
TiO₂	0.25	0.23	0.09	0.12	0.32	0.55	0.49	0.34	0.31
Al₂O₃	15.36	22.77	18.71	20.05	15.77	17.02	16.26	16.29	10.03
FeO	15.35	18.88	15.32	19.94	16.45	14.54	13.65	17.47	11.75
MnO	0.29	0.64	0.63	0.89	0.65	0.42	0.20	0.54	0.30
MgO	10.86	15.39	9.72	13.14	11.76	14.48	12.44	12.26	19.51
CaO	10.56	0.13	5.74	1.54	9.19	5.30	0.05	7.34	6.40
Na₂O	1.20	0.06	0.83	0.03	0.69	1.28	0.49	0.97	0.00
K₂O	0.21	2.15	1.52	0.56	0.18	1.92	5.30	0.11	0.18
H₂O	1.40	5.12	2.96	3.31	2.21	4.01	4.61	2.21	4.27

Table 2. Estimated bulk compositions of each sample made using petrographically estimated modes, analyses from SEM, and idealized Fe-chlorite formula ((Fe)₆AlSi₃O₁₀(OH)₈). RIP4C was estimated using modes of idealized chlorite and albite.

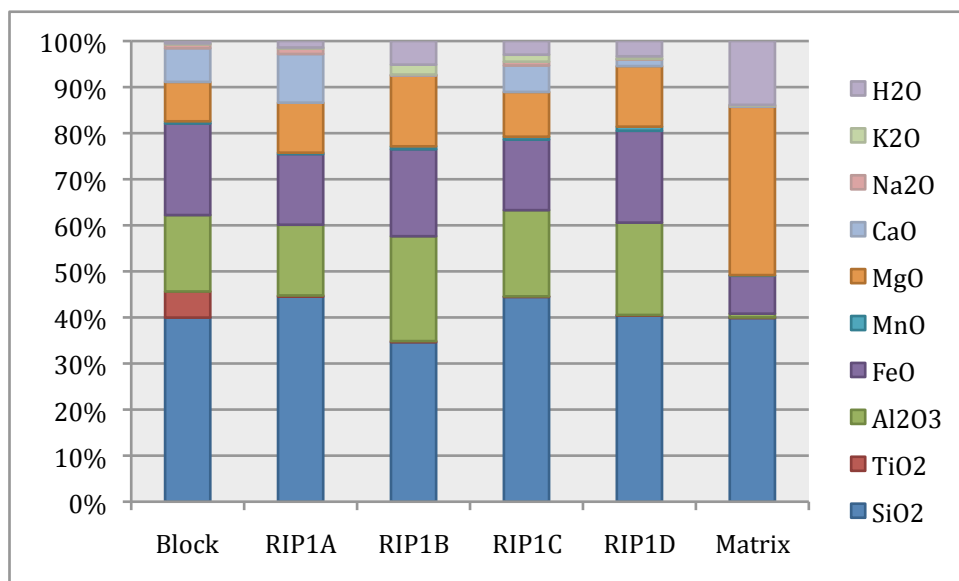


Figure 53. Bulk compositions of sample RIP1A, B, C, and D estimated using mode and chemical analyses as well as idealized chemical formulas for chlorite where necessary. Block and matrix bulk chemistry from Sorensen 1989.

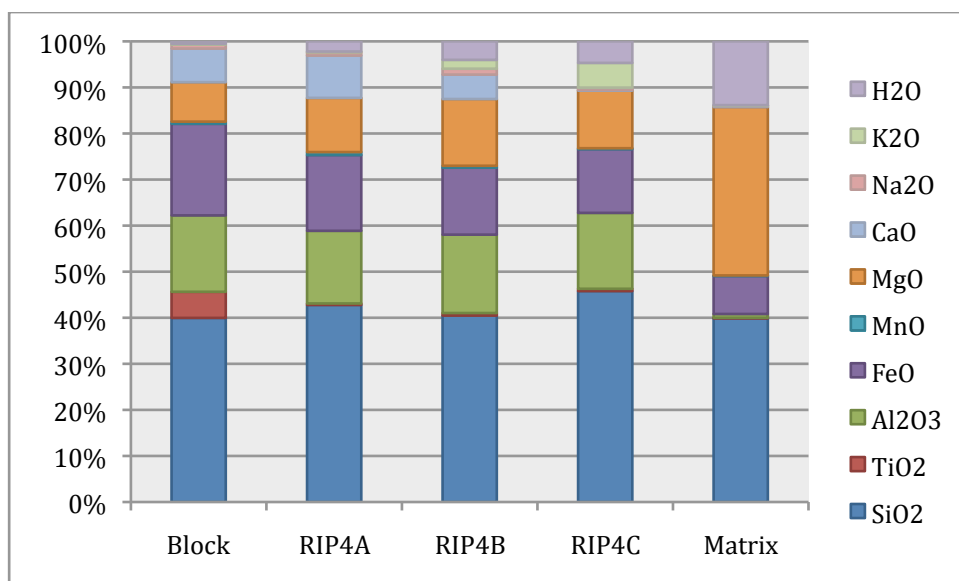


Figure 54. Bulk compositions of sample RIP4A, B, and C estimated using mode and chemical analyses as well as idealized chemical formulas for chlorite where necessary. Block and matrix bulk chemistry from Sorensen 1989.

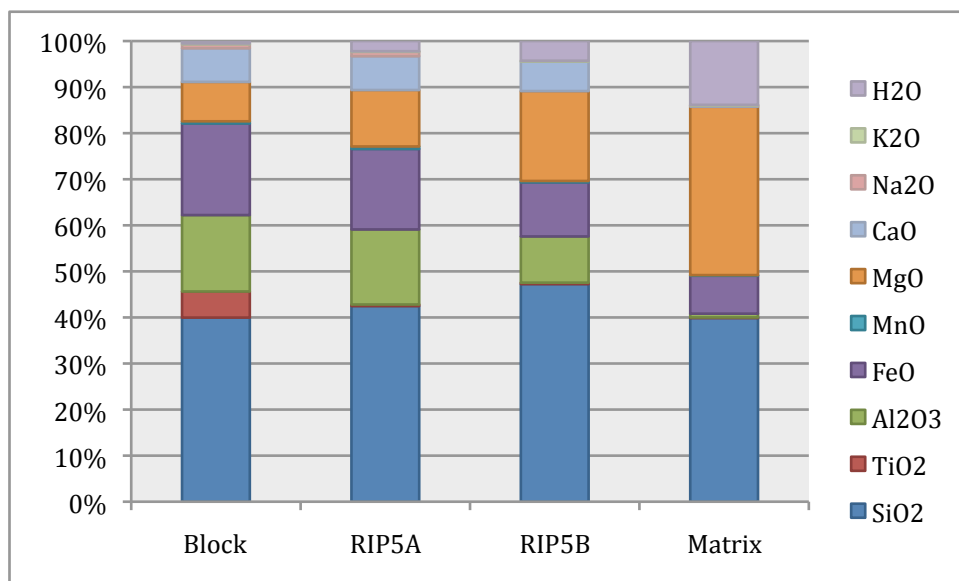


Figure 55. Bulk compositions of sample RIP5A and B estimated using mode and chemical analyses as well as idealized chemical formulas for chlorite where necessary. Block and matrix bulk chemistry from Sorensen 1989.

Thermometry

Application of garnet-hornblende thermometry (Ravna et al., 2000) yields temperatures of 205°C using the garnet core compositions, and 216°C using the garnet rim compositions, both paired with hornblende matrix compositions of sample RIP1A. Other block garnet-hornblende chemistry pairs and rind garnet-hornblende chemistry pairs yielded similarly low temperatures in the 200-350°C range, lower than the threshold of the thermometer (515 °C).

Discussion

Detailed examination of the mineralogy and chemistry of the samples support a model of high temperature amphibolite blocks reacting with a contrasting serpentinite matrix at lower temperatures in the presence of a water-rich fluid. The overall path of the chemical changes during rind formation are indicated in Figure 56, an ACF mineral

assemblage diagram that shows the bulk compositions of the block and matrix along with the compositions the observed minerals.

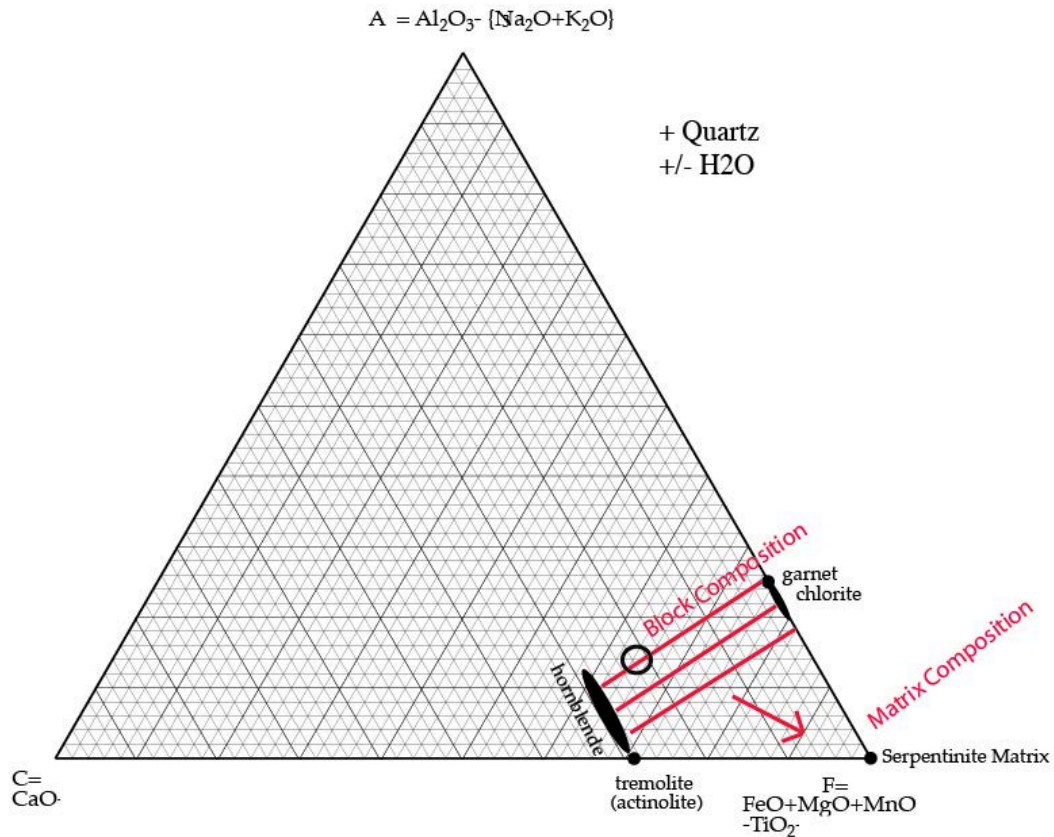
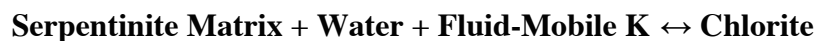


Figure 56. ACF diagram showing rind-forming chemical reaction between block composition toward serpentinite-rich matrix composition. An original assemblage of garnet-hornblende moves toward an actinolite-chlorite assemblage.

Idealized Rind-Forming Reaction:



The block nature of the samples collected in the field suggests that these amphibolites were likely exposed to subduction conditions. Blocks on Ripper's Cove range in size from one meter in diameter to ten meters in diameter, all with a rounded or semi-rounded structure recording a history of being uplifted and ground with matrix. These blocks were broken off their source bedrock formation by the friction of faulting and movement along the subduction zone environment. Continued movement of the subduction faults fully incorporated the block into the *mélange*. Although the mineral assemblage within the blocks suggest higher facies than blueschist, it is evident that these rocks have been through the conveyor belt of a subduction zone.

As previously stated, the mineral assemblage of the samples suggests amphibolite-facies. Although plagioclase, characteristic of the amphibolite facies, is absent, previous work describes a partial-melting period is responsible for its removal and it is widely accepted that such blocks from Catalina Island are amphibolitic, and formed at conditions consistent with the amphibolite-facies (Sorensen 1987). Block assemblages of garnet and amphibole record such high-temperature reactions.

Garnets exchange elements less readily than amphiboles because of their dense crystal structure. The amphibole crystal framework is characterized by larger gaps between planes of atoms. Therefore, garnet chemical compositions are not likely to change at lower temperatures (<700 °C), so garnet compositions are likely to represent primary, high temperature growth compositions. Amphibole compositions, however, may represent lower-temperature diffusional exchange. Comparing both gives insight in whether the block and rind layers began as the same material (Fig. 51, 52).

Past work (e.g. Penniston-Dorland) has suggested that garnets grew after mechanical mixing between garnet-amphibolite blocks and matrix material, followed by

fluid infiltration that caused the retrograde growth of chlorite. The second part of this hypothesis is supported here by a higher concentration of chlorite in exterior rind layers, where water flowing through the matrix would have easier access due to the permeability of the ground-up serpentinite matrix material. Similarity in garnet chemical compositions, both rim and core in both block and rind (Fig. 51), indicate that all garnets likely grew at the same time and in relatively unchanging conditions. This indicates that the rinds are formed by altering block material, rather than from the matrix. Furthermore, eclogite-facies minerals such as clinopyroxene and zoisite ($\text{Ca}_2\text{Al}_3(\text{SiO}_4)_3(\text{OH})$) as inclusions in garnet record a history of eclogite-facies conditions in all block samples. This indicates that the garnets grew, simultaneously, after an initial eclogite-facies reaction had occurred.

Metamorphism of Protolith:



Rind layers are generally composed of actinolite ($\text{Ca}_2(\text{Mg,Fe})_5\text{Si}_8\text{O}_{22}(\text{OH})_{22}$) (Fig. 53), chlorite ($(\text{Mg,Fe,Li})_6\text{AlSi}_3\text{O}_{10}(\text{OH})_8$), phengite ($\text{K}(\text{AlMg})_2(\text{OH})_2(\text{SiAl})_4\text{O}_{10}$), and in one case, RIP4C, albite ($\text{NaAlSi}_3\text{O}_8$) is present (Fig. 54). This indicates that rinds developed at lower temperature than amphibolite facies and lower pressure than blueschist facies, supported by the presence of greenschist-facies minerals. Evidence for lower temperatures in rind minerals suggest that all garnets grew pre-rind formation, which is supported by the similar chemical composition of the garnets.

Because the garnet composition and some of the amphibolite blocks studied by others show that Catalina block garnets formed at high ($>700^\circ\text{C}$) (Towbin 2013) temperatures, block garnets should have been in equilibrium with block hornblendes.

This is due to the rapid kinetic nature of reaction at high temperatures. However, garnet-hornblende thermometry yielded temperatures lower than those necessary to form such garnet-amphibolite blocks. This disparity in temperature indicates a lack of equilibrium between the observed amphibole and garnet compositions, suggests alteration of amphiboles but not garnets during rind formation. This means that the garnet compositions have likely not changed much. In other words, hornblende compositions, even inside the blocks, have been altered since high temperature garnet-forming conditions. Conversely, the geothermometer equation may have been calibrated for different garnet and hornblende compositions, as the abstract suggests the thermometer only works at temperatures above 515 °C and pressure above 5 kbar (Ravna 2000).

Bulk composition chemistry across block and rind layers revealed a gradient consistent with chemical diffusion between two chemically disparate substances, block and matrix. Concentrations of aluminum, iron, and calcium are all greater in the bulk composition of the block, while magnesium is greater in the bulk composition of the matrix (see also Sorensen 1989). The formation of rinds from these two materials should follow a pattern of increasing magnesium in the rind layers and decreasing aluminum, iron, and calcium as one moves out from block toward matrix. Patterns in observed block-rind bulk chemistry differences support such a reaction. Magnesium increases away from the block for all samples, consistent with a magnesium-rich matrix contingent to a block. Calcium decreases slightly away from the block, consistent with diffusion from calcium-rich block to rind. Aluminum tends to increase toward block from outer rind layers with the exception of sample RIP1C and RIP5B. Iron also decreases away from the block, except in RIP1, where there are other complications (see RIP1 section below). Sodium and potassium vary per sample, with Na in low concentrations for all

samples and K increase away from the blocks in samples such as RIP4A to RIP4B. Water concentrations increase away from the block in all samples, consistent with the hydrous serpentinite block (See Fig. 12). The two largest differences are the high concentrations of water and magnesium in the serpentinite, both of which are consistently demonstrated through patterns in bulk composition analyses of all samples in this study as increases of Mg and H₂O from block to rind layer.

Phengite, a potassium-rich mica, is evidence for fluid-flow within the system, as neither the matrix nor the block is a source of potassium (Table 1, Fig. 12). This added component of the system must have been introduced through potassium-bearing fluids flowing around the blocks. This is supported by the presence of phengite in the outermost layers of block + rind samples, e.g. RIP4C.

RIP1

Sample RIP1 is the only case in which garnets exist in a rind layer not directly adjacent to the block (e.g. not in RIP1B, but in RIP1C) (Fig. 37). I hypothesize that this sample may be the product of a reaction between two amphibolite blocks and intervening matrix. This is supported by the texture of the rind, with the RIP1C layer found only on one side of the block. This is also supported by similarly high Si, Al, and Ca concentrations for block layer A and “rind” layer C while layers B and D show lower concentrations. An opposite relationship is true for Fe. In all cases, RIP1A and RIP1C are more chemically similar than RIP1C with rind layers B or D, supporting the theory of a second, chemically similar garnet-amphibolite block (Fig. 53).

The difference in size but similar chemistry of garnets in sample RIP1C (Fig. 32, 33, 34) may also indicate the presence of a separate block. Smaller garnets appear to be

concentrated in quartz vein-like sections rather than garnet amphibolite, which could be a textural feature preserved from the original garnet-amphibolite pre-subduction zone, reaction, or rind formation. The size of the garnets could be attributed to variations in the original basaltic protolith. These variations are absent in RIP1A, suggesting the two were metamorphosed from different pieces of basalt.

RIP4

RIP4C is a sample composed mostly of chlorite, phengite, albite, and quartz (Fig. 44), indicative of both hydration reactions, and introduction of potassium, and greenschist facies temperatures and pressures. Because this sample is characterized by more than one rind and by garnets of equal composition in more than one layer, it appears that the formation of this rind sequence is more complex than the simple block-matrix reaction of RIP5. layers. An increase in magnesium and a decrease in calcium from RIP4A to 4B is consistent with a reaction between block and matrix. However, rind layer RIP4C differs in chemistry sharply and was likely exposed to a larger volume of fluid in the system, introducing a lot of potassium to form phengite mica (Fig. 53).

RIP5

Sample RIP5 is composed of a garnet+hornblende+phengite block and actinolite+chlorite rind (Fig. 50). Chemically, the sample follows a pattern of increasing hydration and magnesium from A to B layers and decreasing aluminum and calcium from A to B layers (Fig. 54). These factors fit a model of a diffusion reaction between block and matrix material. The presence of phengite in the block suggests some infiltration of potassium-bearing fluid into the garnet-amphibolite material.

Conclusions

In conclusion, mechanical mixing, as suggested by previous studies on the Catalina Schist, cannot explain the presence of multiple rind layers. I propose that these blocks were metamorphosed first to eclogite facies (because of omphacite inclusions) and then amphibolite facies with a partial melting episode because of the absence of plagioclase. The blocks were then broken by faulting and moved into the subduction zone complex and introduced to a *mélange* environment. Reactions with serpentinite matrix at lower temperatures and pressures, along with fluid exposure, allowed diffusion reactions of the exterior of garnet-amphibolite blocks to form multiple rind layers in some cases, and single rind layers in others, with greenschist facies minerals.

Future work on these rocks might include an analysis of trace element zoning throughout individual crystal grains and rind layers to define in more detail the diffusion alteration. Additionally, an examination of quartz fluid inclusions found in the rind layer of sample RIP1D could give evidence regarding the chemical composition of fluids that may have altered the system.

References

- Bebout, G.E., and Barton, M.D., 1989. Fluid flow and metasomatism in a subduction zone hydrothermal system: Catalina Schist Terrain, California. *Geology*, 17: 976-980.
- Bebout, Gray. "Metasomatism in Subduction Zones of Subducted Ocean Slabs, Mantle Wedges, and the Slab-Mantle Interface." *Metasomatism and the Chemical Transformation of Rock: The Role of Fluids in Terrestrial and Extraterrestrial Processes*. By Daniel E. Harlov and H. Austrheim. Berlin: Springer, 2012. 289.
- Bube, R. H., F. Herman, and H. W. Leverenz. 1954. "The Solid State." *Annual Review of Physical Chemistry* 5.1: 199-214.
- Brady, J. (1977) "Metasomatic Zones in Metamorphic Rocks." *Geochimica Et Cosmochimica Acta* 41.1: 113-25.
- Brown, G. C., and A. E. Mussett. 1993. *The Inaccessible Earth: An Integrated View to Its Structure and Composition*. London: Chapman & Hall.
- Cherniak, D. J., and A. Dimanov. 2010. "Diffusion in Pyroxene, Mica and Amphibole." *Reviews in Mineralogy and Geochemistry* 72.1: 641-90.
- Dohmen, R., and R. Milke. 2010. "Diffusion in Polycrystalline Materials: Grain Boundaries, Mathematical Models, and Experimental Data." *Reviews in Mineralogy and Geochemistry* 72.1. 921-70.
- Ernst, W. G. 1976. *Petrologic Phase Equilibria*. San Francisco: W.H. Freeman. Print.
- Foster, Robert J. 1988. *General Geology*. Columbus: Merrill Pub., Print.
- Grove, M., et al 2008. The Catalina Schist: Evidence for middle Cretaceous

- subduction erosion of southwestern North America. GSA special paper 436.
- Nesse, William D. 2009. *Introduction to Mineralogy*. New York: Oxford UP. Print.
- Penniston-Dorland et al, 2012. Lithium and its isotopes as tracers of subduction zone fluids and metamorphic processes: Evidence from the Catalina Schist, California, USA. *Geochimica et Cosmochimica Acta* 77. 530-545.
- Ravna, E. J. K., 2000, Distribution of Fe²⁺ and Mg between coexisting garnet and hornblende in synthetic and natural systems: An empirical calibration of the garnet-hornblende Fe-Mg geothermometer: *Lithos*, v.53, p. 265–277.
- Platt, J., 1975, Metamorphic and deformational processes in the Franciscan Complex, California: some insights from the Catalina Schist terrain: *Bulletin of the Geological Society of America*, v. 86, p. 1337–1347.
- Sorensen, S., and Barton, M., 1987, Metasomatism and Partial Melting in a Subduction Complex - Catalina Schist, Southern-California: *Geology*, v. 15, no. 2, p. 115–118.
- Towbin, W. Henry. 2013. *Thermobarometric Modeling of the Catalina Amphibolite Unit: Implications for Tectonic and Metasomatic Models*. Thesis. Oberlin College.
N.p.: n.p., n.d.

Appendix

Elem	RIP1C Small Garnet 1		RIP1C Small Garnet 2		RIP1C Small Garnet 3		RIP1C Garnet 1 Core		RIP1C Garnet 1 Rim		
	Wt %	Mol %	Wt %	Mol %	Wt %	Mol %	Wt %	Mol %	Wt %	Mol %	
MgO	6.5	10.73	6.76	11.23	6.55	10.87	4.85	7.99	7.27	11.89	
Al2O3	22.27	14.53	22.21	14.6	22.06	14.48	21.86	14.26	22.21	14.35	
SiO2	38.88	43.05	38.94	43.43	39.3	43.76	38.44	42.54	39.19	42.97	
CaO	4.33	5.13	3.96	4.73	4.16	4.96	8.22	9.75	5.26	6.17	
MnO	1.74	1.63	1.87	1.77	1.9	1.79	1.81	1.7	1.43	1.33	
FeO	26.93	24.94	26	24.25	25.93	24.14	25.67	23.76	25.4	23.29	
Total	100.6	5	100	99.73	100	99.9	100	100.85	100	100.76	100

Figure A1

Elem	RIP1C Garnet 2 Core		RIP1C Garnet 2 Rim		RIP1C Garnet 3 Core		RIP1C Garnet 3 Rim	
	Wt %	Mol %	Wt %	Mol %	Wt %	Mol %	Wt %	Mol %
MgO	5.53	9.34	6.9	11.48	3.62	6.05	7.41	12.17
Al2O3	20.66	13.79	22.13	14.56	21.38	14.14	22.46	14.59
SiO2	38.96	44.12	38.65	43.14	37.73	42.36	38.86	42.84
CaO	6.54	7.94	4.77	5.7	9.85	11.85	5.05	5.96
MnO	2.24	2.15	1.73	1.63	2.26	2.15	1.48	1.38
FeO	23.94	22.68	25.17	23.49	24.98	23.45	25	23.05
Total	97.87	100	99.35	100	99.82	100	100.25	100

Figure A2

Elem	RIP1A Garnet 1 Core		RIP1A Garnet 1 Rim		RIP1A Garnet 2 Core		RIP1A Garnet 2 Rim		RIP1A Garnet 3 Core		RIP1A Garnet 3 Rim	
	Wt %	Mol %	Wt %	Mol %	Wt %	Mol %	Wt %	Mol %	Wt %	Mol %	Wt %	Mol %
MgO	4.53	7.36	5.82	9.51	2.25	3.74	4.91	8.02	2.93	4.81	5	8.12
Al2O3	22.33	14.33	22.25	14.37	21.66	14.21	22.25	14.36	22.01	14.28	22.05	14.17
SiO2	38.87	42.31	38.7	42.39	38.03	42.33	38.68	42.37	38.53	42.42	38.95	42.48
CaO	9.51	11.09	7.8	9.15	11.45	13.65	9.19	10.78	11.44	13.49	9.5	11.1
MnO	0.99	0.92	0.68	0.63	3.06	2.89	0.58	0.54	1.36	1.27	0.64	0.59
FeO	26.36	24	26.14	23.95	24.91	23.19	26.12	23.93	25.76	23.72	25.81	23.54
Total	102.6	100	101.39	100	101.4	100	101.73	100	102.03	100	101.96	100

Figure A3

Elem	RIP1D Garnet 1 Core		RIP1D Garnet 1 Rim		RIP1D Garnet 2 Core		RIP1D Garnet 2 Rim		RIP1D Garnet 3	
	Wt %	Mol %	Wt %	Mol %	Wt %	Mol %	Wt %	Mol %	Wt %	Mol %
MgO	3.23	5.29	7.4	11.93	5.5	8.79	7.41	11.89	7.46	12.03
Al2O3	22.22	14.38	22.43	14.29	22.37	14.13	22.66	14.38	22.46	14.33
SiO2	38.95	42.77	39.65	42.88	39.79	42.64	40.27	43.36	39.93	43.24
CaO	8.97	10.55	5.56	6.44	7.53	8.64	4.82	5.56	4.75	5.51
MnO	2.02	1.88	1.77	1.62	2	1.81	2.11	1.93	1.98	1.82
FeO	27.36	25.12	25.25	22.84	26.76	23.98	25.42	22.89	25.48	23.07
Total	102.76	100	102.05	100	103.94	100	102.69	100	102.06	100

Figure A4

Elem	RIP4A Garnet 1 Core		RIP4A Garnet 1 Rim		RIP4A Garnet 2 Core		RIP4A Garnet 2 Rim		RIP4B Garnet 1 Rim		RIP4B Garnet 2 Core		RIP4B Garnet 2 Rim			
	Wt %	Mol %	Wt %	Mol %	Wt %	Mol %	Wt %	Mol %	Wt %	Mol %	Wt %	Mol %	Wt %	Mol %	Wt %	Mol %
MgO	2.98	5.18	2.98	5.18	2.42	4.31	5.77	9.96	8.74	14.1	8.89	14.36	9.36	15	9.24	14.83
Al2O3	20.9	14.4	20.9	14.4	20.1	14.2	21.4	14.6	22.4	14.3	22.46	14.35	22.7	14.38	22.85	14.5
SiO2	36.2	42.3	36.2	42.3	35.8	42.8	36.7	42.5	39.8	43.2	39.97	43.33	40.1	43.18	40.03	43.11
CaO	10.1	12.6	10.1	12.6	9.61	12.3	7.92	9.82	4.19	4.87	3.81	4.43	3.96	4.56	3.78	4.36
MnO	1.3	1.29	1.3	1.29	2.02	2.05	0.66	0.64	1.3	1.19	1.3	1.19	1.38	1.26	1.37	1.25
FeO	24.7	24.1	24.7	24.1	24.1	24.2	23.2	22.45	24.51	22.23	24.64	22.3	24.0	21.62	24.38	21.96
Total	96.4	100	96.4	100	94.2	100	95.7	100	101.1	100	101.1	100	101	100	101	100

Figure A5

Elem	RIP5A Garnet 1 Core		RIP5A Garnet 1 Rim		RIP5A Garnet 2 Core		RIP5A Garnet 2 Rim	
	Wt %	%	Wt %	%	Wt %	%	Wt %	%
MgO	7.03	11.42	7.49	12.1	6.72	10.83	7.33	11.79
Al2O3	22.04	14.16	22.59	14.43	22.28	14.21	22.3	14.18
SiO2	39.53	43.07	39.43	42.72	39.74	43	39.67	42.8
CaO	5.63	6.57	5.33	6.19	5.07	5.88	5.03	5.82
MnO	1.08	1.00	0.98	0.9	1.10	1.01	1.15	1.05
FeO	26.09	23.78	26.11	23.66	27.7	25.07	27.00	24.37
Total	101.41	100	101.94	100	102.61	100	102.48	100

Figure A6

Elem	RIP1A Amphibole 1		RIP1A Amphibole 2	
	Wt %	Mole %	Wt %	Mole %
Na2O	1.73	1.65	1.74	1.74
MgO	15.17	22.29	12.84	19.66
Al2O3	11.41	6.63	14.24	8.62
SiO2	49.6	48.9	46.12	47.36
K2O	0.27	0.17	0.34	0.22
CaO	10.85	11.46	10.77	11.86
TiO2	0	0	0.73	0.57
MnO	0	0	0	0
FeO	10.81	8.91	11.63	9.98
Total	99.83	100	98.42	100

Figure A7

Elem	RIP1B Mineral		RIP1B Mineral		RIP1C Amphibole 1		RIP1D Amphibole 1		RIP1D Amphibole 2	
	Wt %	Mole %	Wt %	Mole %	Wt %	Mole %	Wt %	Mole %	Wt %	Mole %
Na2O	1.27	1.25	1.27	1.25	2.3	2.27	2.11	2.49	2.29	2.73
MgO	18	27.23	18	27.23	13.9	21.14	12.02	21.82	11.89	21.81
Al2O3	7.19	4.3	7.19	4.3	14.53	8.74	12.16	8.73	12.53	9.09
SiO2	50.11	50.87	50.11	50.87	47.17	48.12	40.09	48.84	39.15	48.2
K2O	0.16	0.1	0.16	0.1	0	0	0.24	0.19	0.26	0.2
CaO	10.3	11.2	10.3	11.2	10.04	10.97	8.42	10.99	8.36	11.02
TiO2	0.38	0.29	0.38	0.29	0	0	0.5	0.46	0.69	0.64
MnO	0	0	0	0	0	0	0.27	0.28	0.24	0.25
FeO	7.02	5.52	5.6	4.76	10.26	8.75	6.09	6.2	5.88	6.05
Total	100.86	100	93.01	100	98.2	100	81.9	100	81.29	100

Figure A8

Elem	RIP4A Amphibole 1		RIP4A Amphibole 2		RIP4B Amphibole 1		RIP5A Amphibole 1		RIP5A Amphibole 2	
	Wt %	Mole %								
Na2O	1.37	1.4	1.03	1.05	2.59	2.51	1.96	1.89	1.61	1.55
MgO	14.57	22.88	14.97	23.5	14.65	21.85	14.86	22.09	15.23	22.54
Al2O3	11.21	6.96	9.52	5.91	15.39	9.07	12.72	7.48	11.54	6.75
SiO2	45.66	48.09	46.67	49.14	47.1	47.14	47.81	47.7	49.01	48.68
K2O	0.31	0.21	0.3	0.2	0.32	0.21	0.23	0.15	0.17	0.11
CaO	10.31	11.63	10.27	11.59	10.04	10.76	10.47	11.19	10.26	10.92
TiO2	0.63	0.5	0.48	0.38	0.79	0.6	0.73	0.55	0.52	0.39
MnO	0.2	0.18	0.17	0.15	0.32	0.27	0.22	0.18	0.2	0.17
FeO	9.26	8.15	9.17	8.07	9.07	7.59	10.51	8.77	10.72	8.91
Total	93.53	100	92.58	100	100.28	100	99.5	100	99.25	100

Figure A9